Electronic Supplementary Information (ESI) for

Concentration–structure dual-gradient architecture in high-Ni/low-Co single-crystal NCM cathodes

Jun Bum Park,‡[a] Minje Ryu,‡[b] Eui-Yeon Jeong,[c] Young Gyun Choi,[d] Sung Hyun Cho,[a] Seok Yun Kim,[b] Byungwook Kang,[e] Kisuk Kang,*[e,f,g] Seong-Min Bak,*[c] and Jong Hyeok Park*[b]

[a.] Department of Battery Conflation Engineering, Yonsei University, 50 Yonsei-ro, Seodaemun-gu, Seoul 03722, Republic of Korea.

[b.] Department of Chemical and Biomolecular Engineering, Yonsei University, 50 Yonsei-ro, Seodaemun-gu, Seoul 03722, Republic of Korea.

[c.] Department of Materials Science and Engineering, Yonsei University, 50 Yonsei-ro, Seodaemun-gu, Seoul 03722, Republic of Korea.

[d.] Advanced Automotive Battery Development Center, LG Energy Solution, 188 Munji-ro, Yuseong-gu, Daejeon 34122, Republic of Korea.

[e.] Department of Materials Science and Engineering, Seoul National University, 1 Gwanak-ro, Gwanak-gu, Seoul 08826, Republic of Korea.

[f.] Institute of Engineering Research, College of Engineering, Seoul National University, 1 Gwanak-ro, Gwanak-gu, Seoul 08826, Republic of Korea.

[g.] Institute for Rechargeable Battery Innovations, Research Institute of Advanced Materials, Seoul National University, 1 Gwanak-ro, Gwanak-gu, Seoul 08826, Republic of Korea.

‡ These authors contributed equally to this work.

* Corresponding authors. E-mail: matlgen1@snu.ac.kr; smbak@yonsei.ac.kr; lutts@yonsei.ac.kr

Experimental Section

Materials synthesis

Co_3O_4 nanoparticles (NPs) were synthesized via a modified thermal decomposition method. First, 29.6 g of cobalt nitrate hexahydrate ($Co(NO_3)_2 \cdot 6H_2O$, JUNSEI, Japan, ≥ 98.0%) was dissolved in 300 mL of 1-hexanol ($CH_3(CH_2)_5OH$, SAMCHUN, Korea, 98.0%) under stirring at 900 rpm for 1 h. Subsequently, 21.6 g of oleylamine ($C_{18}H_{35}NH_2$, TCI, Japan, > 50.0%) was added, and the solution was heated to 120 °C with continuous stirring, under reflux conditions. After the solution turned purple, 42 g of deionized water was added dropwise, and the reaction proceeded for 2 h. Upon completion, the mixture turned black and was cooled naturally to room temperature. The resulting Co_3O_4 NPs were collected by centrifugation and washed twice with 1-hexanol and acetone to remove residual oleylamine. The final product was dried overnight at 60 °C in a vacuum oven.

Co-coated NCM (C-NCM) cathode was prepared via a dry coating process followed by post-annealing. Commercial single-crystal NCM960103 ($LiNi_{0.96}Co_{0.01}Mn_{0.03}O_2$, L&F, Korea, D_{50} ≈ 3.18 μm) was used as bare NCM (B-NCM) cathode, and pre-synthesized Co_3O_4 NPs were employed as coating material. A lab-scale high-energy mixer (Spheric Coater, KM Tech, Korea) was used for the dry coating process. Initially, B-NCM powders were pre-blended with specific amounts (0.5 to 2.0 wt.% of cathode weight) of Co_3O_4 NPs to ensure homogeneous distribution of the coating material. For the preparation of C-NCM cathode, an optimal amount of 1.0 wt.% was selected. The mixture was then transferred to the high-energy mixer, and dry coated at 4000 rpm for 20 min. This product was denoted as intermediate NCM (I-NCM) cathode. Finally, I-NCM powders were post-annealed at 720 °C for 5 h under O_2 flow to obtain C-NCM cathode. For clarity, the sample definitions are summarized in Table S1 (ESI†).

Table S1 Summary of sample definitions for B-NCM, I-NCM, and C-NCM cathodes.

Sample	Cathode active material	Coating material and its content	Dry coating conditions	Post-annealing conditions
B-NCM	$LiNi_{0.96}Co_{0.01}Mn_{0.03}O_2$	-	-	-
I-NCM	$LiNi_{0.96}Co_{0.01}Mn_{0.03}O_2$	Co_3O_4 NPs, 1.0 wt.%	4000 rpm, 20 min	-
C-NCM	$LiNi_{0.96}Co_{0.01}Mn_{0.03}O_2$	Co_3O_4 NPs, 1.0 wt.%	4000 rpm, 20 min	720 °C, 5 h, O_2 flow

Materials characterization

Crystal structures of NCM cathodes and Co_3O_4 NPs were analyzed by high-resolution X-ray diffraction (HRXRD, SmartLab, Rigaku, Japan) using Cu Kα radiation (λ = 1.5406 Å) at a scan rate of 1.2° min^{-1} over a 2θ range of 5-140°. For pristine C-NCM cathode, synchrotron-based HRXRD was performed at the 9B High-Resolution Powder Diffraction (HRPD) beamline (λ = 1.5460 Å) of the PLS-II synchrotron radiation facility (Pohang, Korea). Pristine powders were

loaded into a flat airtight sample holder to minimize air exposure during measurement. HRXRD patterns were collected over a 2θ range of 10-130° at a scan rate of 0.01° s^{-1}. Rietveld refinements were conducted using the GSAS-II software package to obtain detailed crystallographic information. Surface and cross-sectional morphologies of the cathodes and coating material were examined by scanning electron microscopy (SEM, JSM-7800F, JEOL, Japan). Cross-sectional samples of NCM electrodes were prepared using an ion beam cross-section polisher (CP, IB-19510CP, JEOL, Japan). Elemental compositions (Li, Ni, Co, and Mn) of the NCM cathodes and dissolved transition-metals (Ni, Co, and Mn) on the cycled Li metal surface were quantified using inductively coupled plasma optical emission spectroscopy (ICP-OES, 5110, Agilent, USA). Residual lithium content and pH of NCM cathodes were measured by an acid–base titration method. 5 g of cathode powder was dispersed in 100 mL of deionized water (solid-to-liquid ratio = 1 : 20, w/v), stirred for 5 min, and vacuum filtered using a qualitative filter paper (Grade F1002, 55 mm, CHMLab, Spain) and a vacuum filtration assembly (47 mm, DURAN, Germany). Subsequently, 50 mL of the filtrate was titrated with 0.1 M HCl using an automatic titrator (904 Titrando, Metrohm, Switzerland). Each sample was independently measured three times for pH and residual lithium content (LiOH and Li_2CO_3), and the averaged values were used. Detailed calculation method for residual lithium content has been described in previous reports.[9,30] X-ray photoelectron spectroscopy (XPS, K-Alpha, Thermo Fisher Scientific, USA) was conducted to investigate the surface chemical states of cathode particles. All binding energies were calibrated with reference to the C 1s peak of adventitious carbon at 284.8 eV. Microstructure and crystal lattice of cathode samples were analyzed by high-resolution transmission electron microscopy (HRTEM, JEM-ARM200F, JEOL, Japan) after preparing cross-sectional samples using a focused ion beam (FIB, Crossbeam 350, ZEISS, Germany). Elemental (Ni, Co, Mn, and O) and structural distributions within the particles were examined using energy-dispersive X-ray spectroscopy (EDS) and fast Fourier transform (FFT) techniques. Electron energy loss spectroscopy (EELS) at the Co L-, Ni L-, and O K-edges was conducted using scanning transmission electron microscopy (STEM, JEM-ARM200F, JEOL, Japan) to elucidate surface-to-bulk electronic structure variations in cathode particles. Focused ion beam (FIB, Helios G4, Thermo Fisher Scientific, USA) was also employed for STEM-EELS sample preparation. Soft X-ray absorption spectroscopy (soft XAS) at the Co L-edge was conducted on pristine C-NCM cathode to examine the Co oxidation state of the surface Co-rich coating layer. Measurements were performed at the 10D XAS_KIST beamline of the PLS-II synchrotron radiation facility (Pohang, Korea). Reference $LiCoO_2$ and CoO samples were prepared by a conventional slurry-casting method using Al foil as the substrate. All spectra were collected in total electron yield (TEY) mode (probing depth ≤ 10 nm) to selectively obtain surface-sensitive information, with a spectral resolution of 0.1 eV under ultra-high vacuum conditions. Atomic force microscopy (AFM, NX10, Park Systems, Korea) was conducted in scanning spreading resistance microscopy (SSRM) mode in a glove box to map current distributions within NCM electrodes. Measurements were performed in PinPoint mode with a scan size of 20 μm × 20 μm (256 × 256 pixels, spatial resolution < 80 nm) using a diamond-coated conductive cantilever (AD-40-AS, Bruker, USA) at +3 V sample bias. Cross-sectional samples for SSRM-AFM were prepared using an ion

milling system (ArBlade 5000, Hitachi High-Tech, Japan) in an inert atmosphere to prevent formation of resistive impurity layers. Four-point probe resistivity measurements (CMT-100J, AIT, Korea) were conducted to evaluate the sheet resistance of NCM electrodes. Measurements were conducted on two independently prepared electrodes per sample, with three repeated measurements on each electrode (n = 6). The mean and standard deviation (s.d.) were calculated from all six measurements. An electrode resistance measurement system (XF057, HIOKI, Japan) was used to evaluate the composite resistance and contact resistance of NCM electrodes. Measurements were conducted on three independently prepared electrodes per sample, with three repeated measurements on each electrode (n = 9). The mean and standard deviation (s.d.) were calculated from all nine measurements. The electrode thickness and areal loading were carefully controlled for the four-point probe resistivity and electrode resistance measurements, and detailed electrode parameters are summarized in Table S8 (ESI†).

Electrochemical characterization

2032-type coin cells were used for the electrochemical analysis. For the preparation of NCM cathodes, carbon black (Super P, Imerys, France) and polyvinylidene fluoride (PVdF, Kynar® HSV900, Arkema, France) were used as conductive additive and binder, respectively. The components (NCM : Super P : PVdF = 94:3:3 wt.%) were dispersed in N-methyl-2-pyrrolidone (NMP, Sigma-Aldrich, USA, anhydrous) and slurry-cast onto Al current collectors. The electrodes were dried in a vacuum oven at 110 °C for 6 h and punched into 14 mm-diameter disks. The areal capacity was set to 2.0 mAh cm^{-2} (mass loading ≈ 10.1 mg cm^{-2}). Li metal foil (Honjo Metal, Japan, 200 μm) was punched into 16 mm-diameter disks and used as the counter electrode for the half cell tests. For full cell assembly, artificial graphite (LG Energy Solution, Korea) with styrene-butadiene rubber (SBR, EQ-Lib-SBR, MTI Corporation, USA, 50 wt.% in DI water) and carboxymethyl cellulose (CMC, Sigma-Aldrich, USA) as aqueous binders (graphite : Super P : SBR : CMC = 95:1:2:2 wt.%) was slurry-cast onto Cu current collectors, dried at 80 °C for 12 h, and punched into 15 mm-diameter disks. The N/P ratio was set to 1.2. Polyethylene (PE, T16-518, SK Energy, Korea, 16 μm) separator and 1 M $LiPF_6$ in ethylene carbonate (EC) : diethyl carbonate (DEC) = 1:1 (v/v) with 10 wt.% fluoroethylene carbonate (FEC) electrolyte (PuriEL, Soulbrain, Korea) were used for all electrochemical tests, and cell assembly was carried out in an Ar-filled glove box.

Electrochemical tests were performed using a battery cycler (WBCS 3000, WonATech, Korea) in the constant current–constant voltage (CC–CV) charging mode in the voltage range of 3.0–4.3 V (vs. Li/Li^+) at 25 °C. For the formation step, one precycle at 0.1 C (1.0 C = 210 mA g^{-1}) was conducted for half cells prior to testing. For the discharge rate capability test, cells were charged at a constant rate of 0.2 C and then discharged at rates ranging from 0.2 C to 5.0 C. In the charge rate capability test, cells were discharged at a constant rate of 0.2 C, while the charging rates were varied from 0.2 C to 5.0 C in both constant current (CC) and CC–CV modes. Half cell cycling tests were carried out at charge and discharge rates of 1.0 C. Full cells were cycled at 0.5 C within 2.7–4.3 V (vs. Li/Li^+) after three precycles at 0.1 C. For clarity, the

electrode specifications and electrochemical testing conditions for coin-type half cells and full cells are summarized in Table S2–S3 (ESI†). Differential capacity (dQ/dV) analysis was performed on half cells under 0.5 C cycling within the voltage range of 3.0–4.3 V (vs. Li/Li^+) at 25 °C. Direct current internal resistance (DC-IR) measurements were carried out on half cells. Each cell was first charged and discharged at 0.05 C, then charged to 3.7 V and rested for 1 h. Finally, at increasing C-rates (0.025–3.0 C), the cells were charged for 10 s, rested for 20 min, discharged for 10 s, and rested for 20 min. Electrochemical impedance spectroscopy (EIS) measurements were conducted on fully charged (4.3 V) half cells after 1, 100, and 200 cycles at 1.0 C. Measurements were performed at 25 °C using an electrochemical workstation (ZIVE MP1, WonATech, Korea) with an AC signal of 10 mV over a frequency range of 1 MHz to 0.01 Hz. Distribution of relaxation times (DRT) analysis was further applied to the obtained EIS data using DRTtools software developed by Ciucci et al., which is publicly available on GitHub (https://github.com/ciuccislab/DRTtools). Galvanostatic intermittent titration technique (GITT) measurements were performed on half cells at 25 °C over a voltage range of 3.0–4.3 V. A pulse current of 0.1 C was applied for 10 min, followed by a 1 h relaxation period. To analyze NCM cathodes at highly delithiated states, the 4.3 V charged electrode was prepared by first charging and discharging the cell at 0.1 C and then charging to 4.3 V at the same rate. Post-mortem analysis was conducted on half cells that underwent 200 cycles at 1.0/1.0 C following a 0.1 C formation step. The cells were disassembled in an Ar-filled glove box to collect electrode samples for both analyses.

Table S2 Summary of electrode specifications and electrochemical testing conditions for coin-type half cells.

Cathode	Electrode composition (wt.%)	NCM : Super P : PVdF = 94 : 3 : 3
	Current collector	Al (20 μm)
	Theoretical capacity (mAh g^{-1})	210
	Electrode area (cm^2, 14 mm-diameter disks)	1.539
	Electrode thickness after calendering (μm)	54
	Areal capacity (mAh cm^{-2})	2.0
	Areal mass loading (mg cm^{-2})	10.1
	Electrode coating density (g cm^{-3})	3.0
Anode	Li metal (200 μm)	
Separator	PE (16 μm)	
Electrolyte	1 M $LiPF_6$ in EC : DEC = 1:1 (v/v) + FEC 10 wt.% (100 μL)	
Voltage window	3.0–4.3 V (vs. Li/Li^+)	
Temperature	25 °C	

Formation protocol	CC–CV charge (0.1 C) and CC discharge (0.1 C) for 1 cycle
Discharge C-rate test	CC–CV charge (0.2 C) and CC discharge (0.2–5.0 C)
Charge C-rate test	CC charge (0.2–5.0 C) and CC discharge (0.2 C) CC–CV charge (0.2–5.0 C) and CC discharge (0.2 C)
Cycling test	CC–CV charge (1.0 C) and CC discharge (1.0 C)

Table S3 Summary of electrode specifications and electrochemical testing conditions for coin-type full cells.

Cathode	Electrode composition (wt.%)	NCM : Super P : PVdF = 94 : 3 : 3
	Current collector	Al (20 μm)
	Theoretical capacity (mAh g^{-1})	210
	Electrode area (cm^2, 14 mm-diameter disks)	1.539
	Electrode thickness after calendering (μm)	54
	Areal capacity (mAh cm^{-2})	2.0
	Areal mass loading (mg cm^{-2})	10.1
	Electrode coating density (g cm^{-3})	3.0
Anode	Electrode composition (wt.%)	Graphite : Super P : SBR : CMC = 95 : 1 : 2 : 2
	Current collector	Cu (18 μm)
	Theoretical capacity (mAh g^{-1})	350
	Electrode area (cm^2, 15 mm-diameter disks)	1.767
	Areal capacity (mAh cm^{-2})	2.4
	Areal mass loading (mg cm^{-2})	7.2
N/P ratio	1.2	
Separator	PE (16 μm)	
Electrolyte	1 M $LiPF_6$ in EC : DEC = 1:1 (v/v) + FEC 10 wt.% (100 μL)	
Voltage window	2.7–4.3 V (vs. Li/Li^+)	
Temperature	25 °C	
Formation protocol	CC–CV charge (0.1 C) and CC discharge (0.1 C) for 3 cycles	
Cycling test	CC–CV charge (0.5 C) and CC discharge (0.5 C)	

High-loading dry-processed electrodes were fabricated using a hot-pressing method. The powder mixture of NCM, multi-walled carbon nanotubes (MWCNT, JENOTUBE 10B, JEIO, Korea), Super P, and PVdF (NCM : MWCNT : Super P : PVdF = 95:1.5:1.5:2 wt.%) was placed onto chemically etched Al foil (JCC, Korea, 20 μm) and hot-pressed to produce dry electrodes. The electrodes were punched into 12.9 mm-diameter disks, yielding an areal capacity of 4.6–6.2 mAh cm^{-2} (mass loading ≈ 23.1–31.1 mg cm^{-2}). Detailed fabrication procedures are described in our previous work.[78] For pouch-type half cells, NCM electrodes (NCM : Super P : PVdF = 94:3:3 wt.%, areal capacity = 2.0 mAh cm^{-2}) were punched into 3 cm × 6 cm rectangles (18 cm^2), yielding a cell capacity of 36 mAh. All other components (Li counter electrode, separator, and electrolyte) were identical to those used for coin-type half cells. Electrode air storage test was conducted to evaluate the effect of RLCs accumulation during air exposure. NCM composite electrodes (14 mm in diameter) were stored for 2 weeks in a temperature- and humidity-controlled chamber (JSBI-100CX, JS Research, Korea) maintained at 25 °C and 10% RH under ambient air. The electrodes were placed with the Al current collector facing downward to ensure effective exposure of the composite electrode surface to ambient air. The stored electrodes were then assembled into coin-type half cells for discharge rate capability tests and compared with unexposed electrodes.

To evaluate and compare practical energy density and electrochemical stability, bilayer pouch-type full cells were assembled using either slurry-cast or dry-processed electrodes. The cell configuration was standardized with one double-sided cathode (3 × 3 cm^2) sandwiched between two single-sided anodes (3.2 × 3.2 cm^2), ensuring a 1.0 mm anode overhang on all sides to mitigate lithium plating at the electrode edges. Slurry-cast NCM electrodes were prepared by coating an NMP-based slurry (NCM : Super P : PVdF = 94:3:3 wt.%) onto an Al foil using a doctor blade, followed by vacuum drying at 110 °C for 6 h. The areal capacity per side was set to 2.05 mAh cm^{-2} (mass loading ≈ 10.4 mg cm^{-2}), corresponding to a total areal capacity of 4.1 mAh cm^{-2} (mass loading ≈ 20.8 mg cm^{-2}). In contrast, a dry-processed cathode was fabricated using a solvent-free powder mixture of NCM, MWCNT, Super P, and PVdF (95:1.5:1.5:2 wt.%). This mixture was homogenized via high-shear vortex mixing and hot-press coated at 180 °C onto a chemically etched Al current collector. This step was repeated on the reverse side to form a double-sided dry electrode, adapting the procedure from our previous work.[78] The areal capacity per side was set to 4.05 mAh cm^{-2} (mass loading ≈ 20.3 mg cm^{-2}), corresponding to a total areal capacity of 8.1 mAh cm^{-2} (mass loading ≈ 40.6 mg cm^{-2}). For both cases, slurry-cast graphite anodes (graphite : Super P : SBR : CMC = 95:1:2:2 wt.%) coated on Cu current collectors were employed as the counter electrodes. The anode mass loading was adjusted for each case to precisely control the N/P ratio, targeting 1.06 and 1.08 for the slurry-cast and dry-processed NCM cathodes, respectively. After placing a polyethylene (PE) separator between the electrodes, the stacked assembly was encapsulated in an Al laminated pouch. A 1 M $LiPF_6$ in EC : DEC = 1:1 (v/v) with 10 wt.% FEC was used as the electrolyte, and a lean-electrolyte condition (E/C ≈ 1.23 g Ah^{-1}) was maintained to maximize the cell-level energy density. Finally, the cells were vacuum-sealed and aged for 12 h to ensure sufficient electrolyte wetting prior to electrochemical characterization. Detailed specifications of the bilayer pouch-type full cell, along with the methods used to calculate the

volumetric and specific energy densities, are provided in Table S13–S14 (ESI†). The slurry-cast electrodes were subjected to three formation cycles at 0.1 C, followed by cycling at 1.0 C. In contrast, the dry-processed electrode underwent one formation cycle at 0.05 C and three cycles at 0.1 C, followed by cycling at 0.5 C. All tests were conducted at 25 °C within a voltage window of 2.7–4.3 V (vs. Li/Li^+).

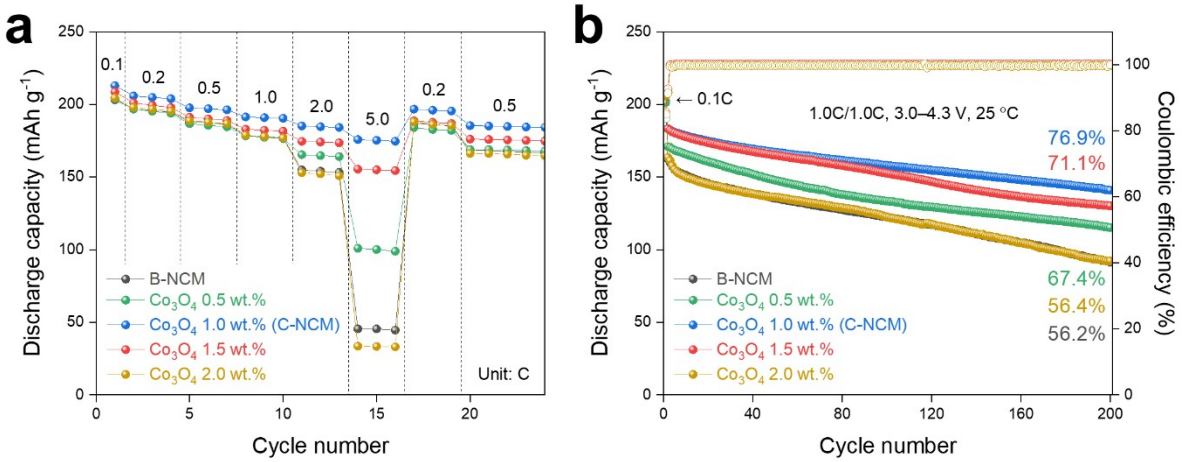

Fig. S1 Co_3O_4 nanoparticles (coating material) content optimization based on (a) rate capability and (b) cycling test. All tests were conducted at 25 °C within a voltage window of 3.0–4.3 V.

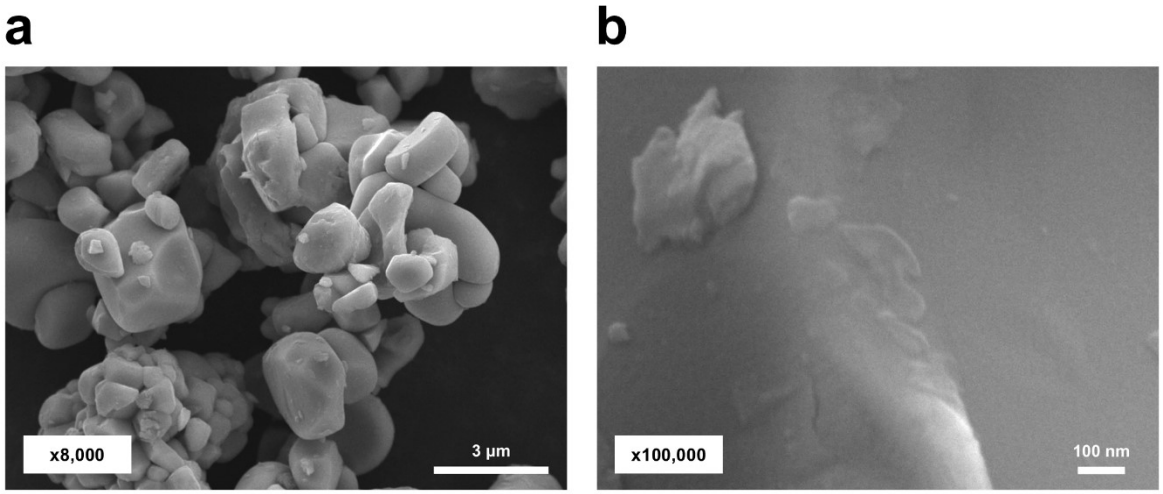

Fig. S2 (a) Low magnification (×8,000) and (b) high magnification (×100,000) SEM images of B-NCM cathode particles.

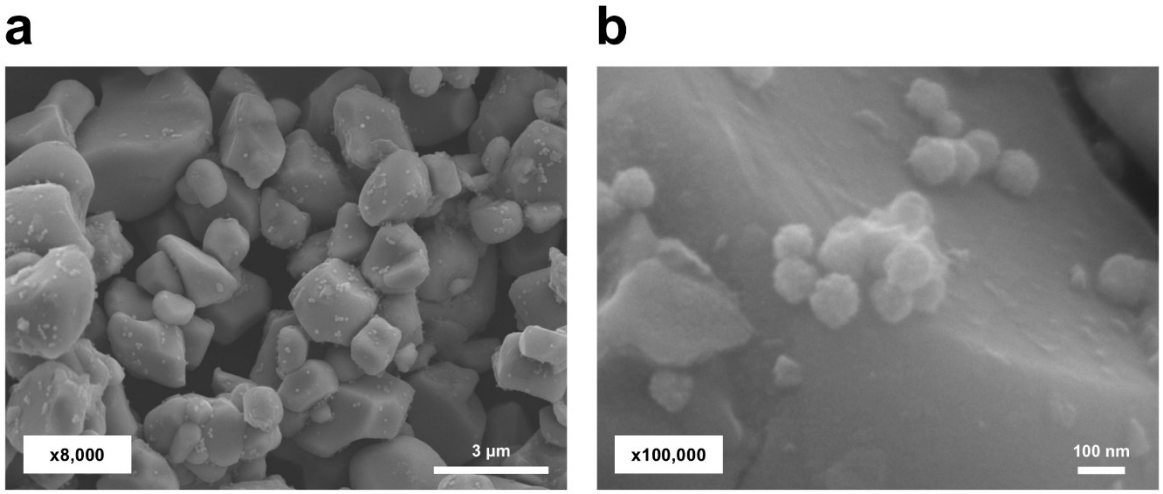

Fig. S3 (a) Low magnification (×8,000) and (b) high magnification (×100,000) SEM images of I-NCM cathode particles.

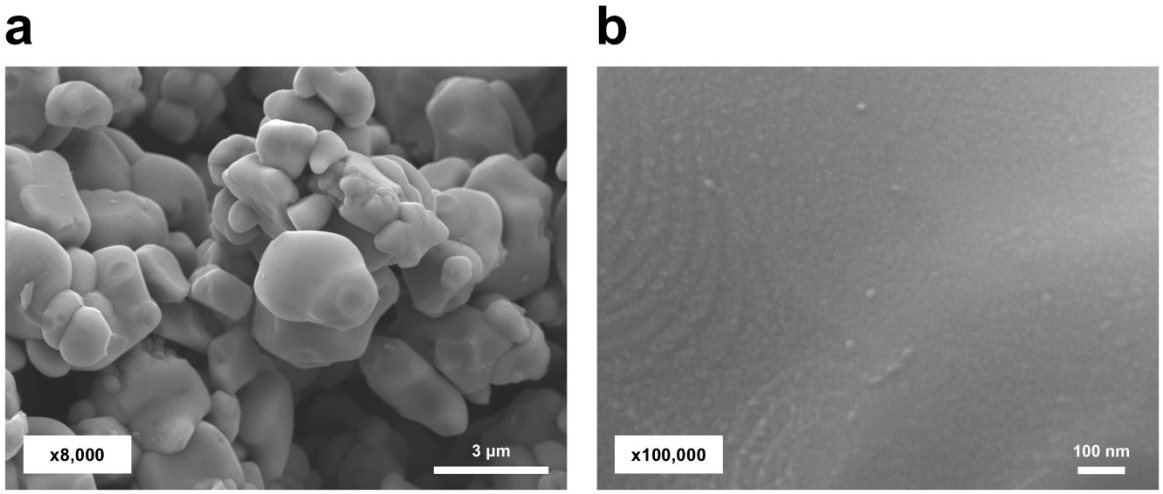

Fig. S4 (a) Low magnification (×8,000) and (b) high magnification (×100,000) SEM images of C-NCM cathode particles.

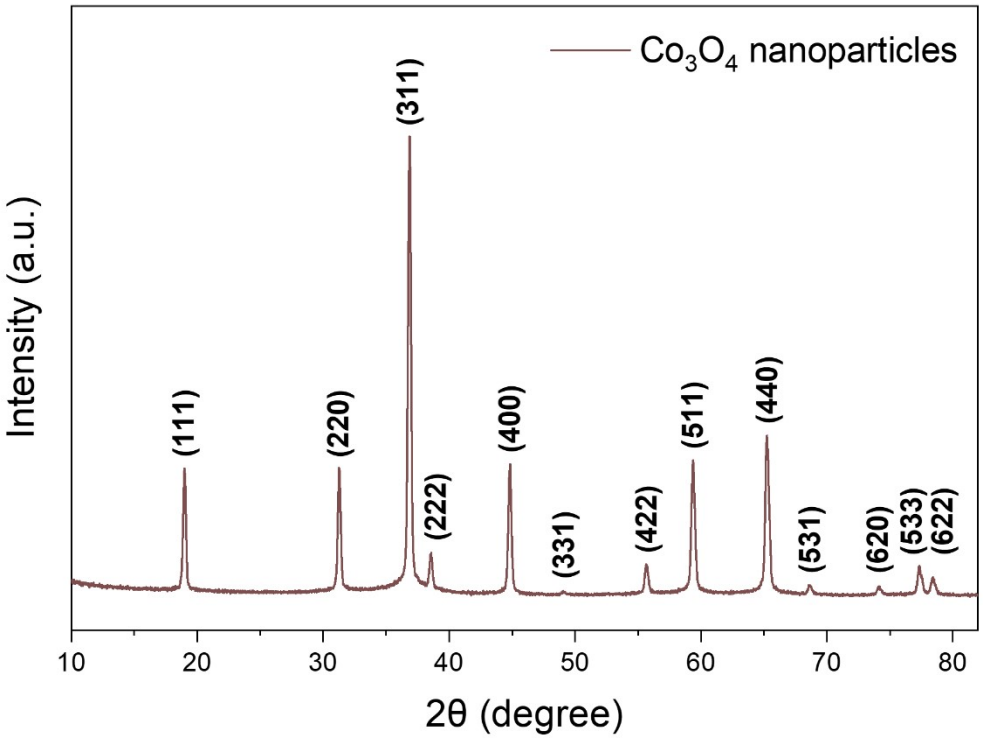

Fig. S5 HRXRD pattern of Co_3O_4 nanoparticles (Cu Kα radiation, λ = 1.5406 Å).

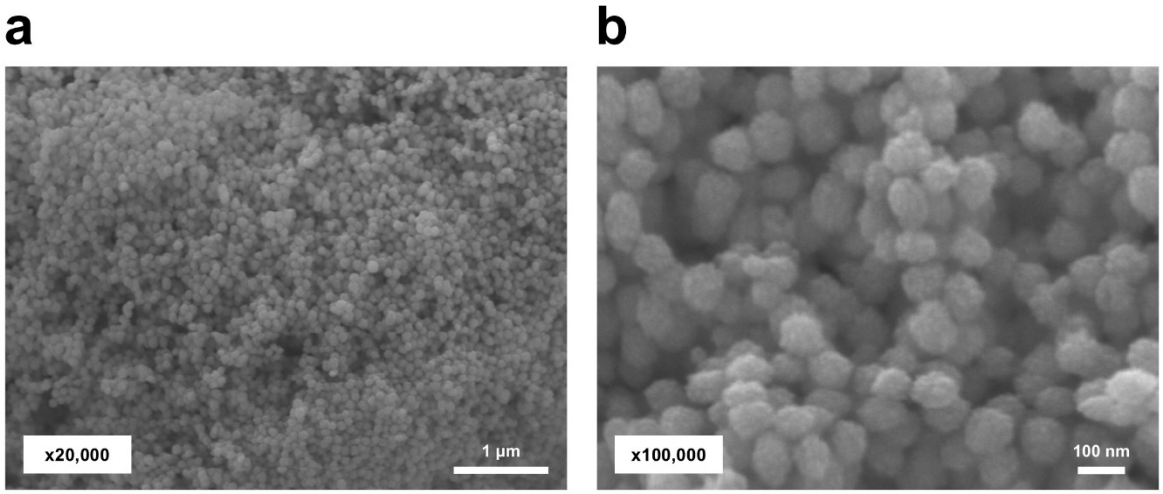

Fig. S6 (a) Low magnification (×20,000) and (b) high magnification (×100,000) SEM images of Co_3O_4 nanoparticles.

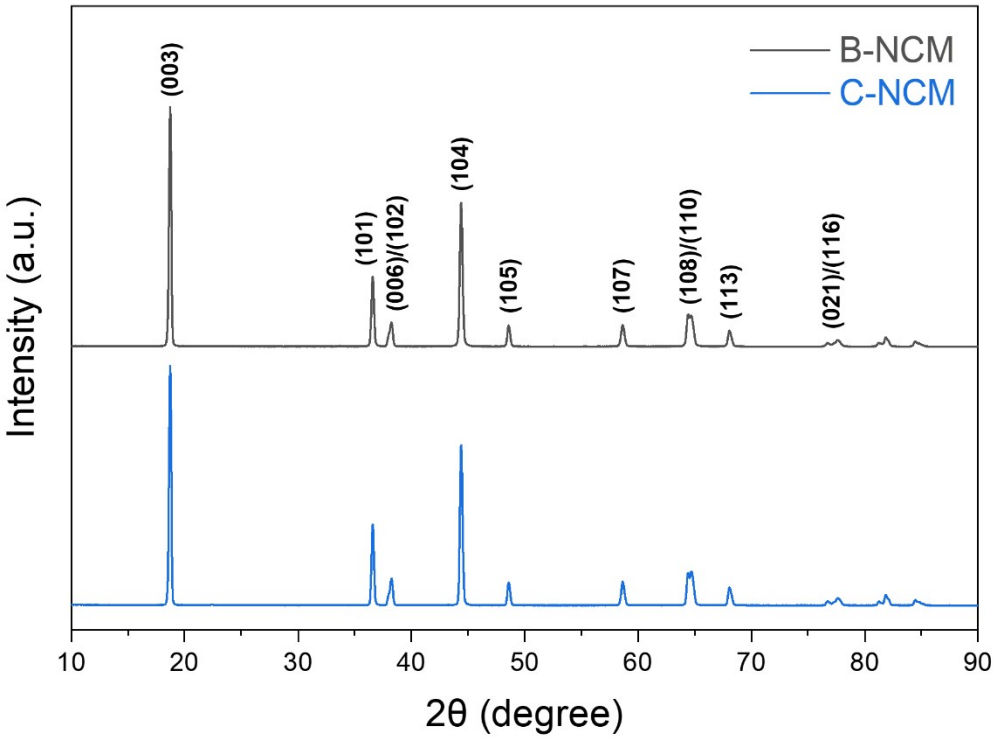

Fig. S7 HRXRD patterns of B-NCM and C-NCM cathodes (Cu Kα radiation, λ = 1.5406 Å).

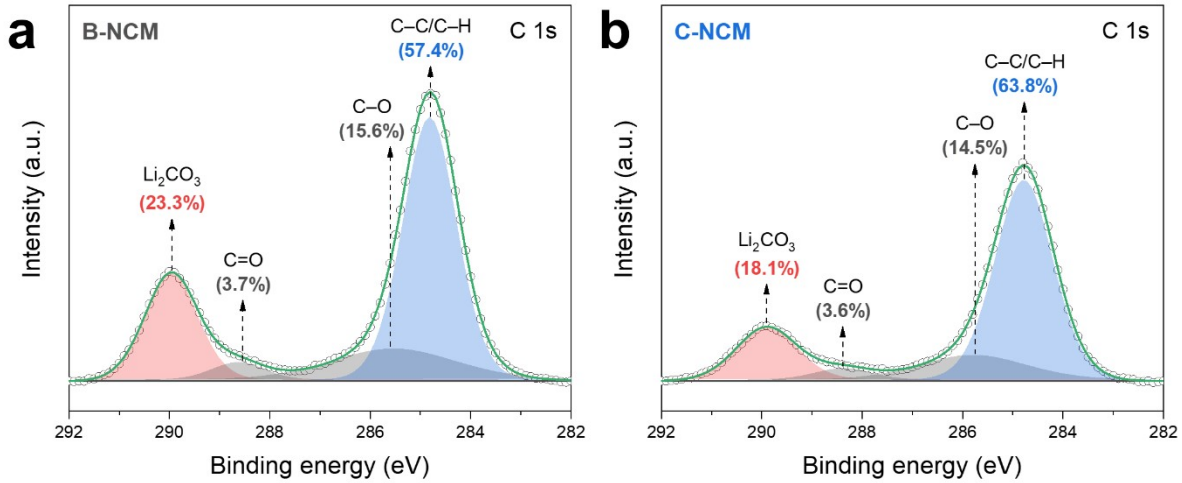

Fig. S8 C 1s XPS spectra collected from the surface of pristine (a) B-NCM and (b) C-NCM cathodes (surface-sensitive mode, probing depth ≤ 10 nm).

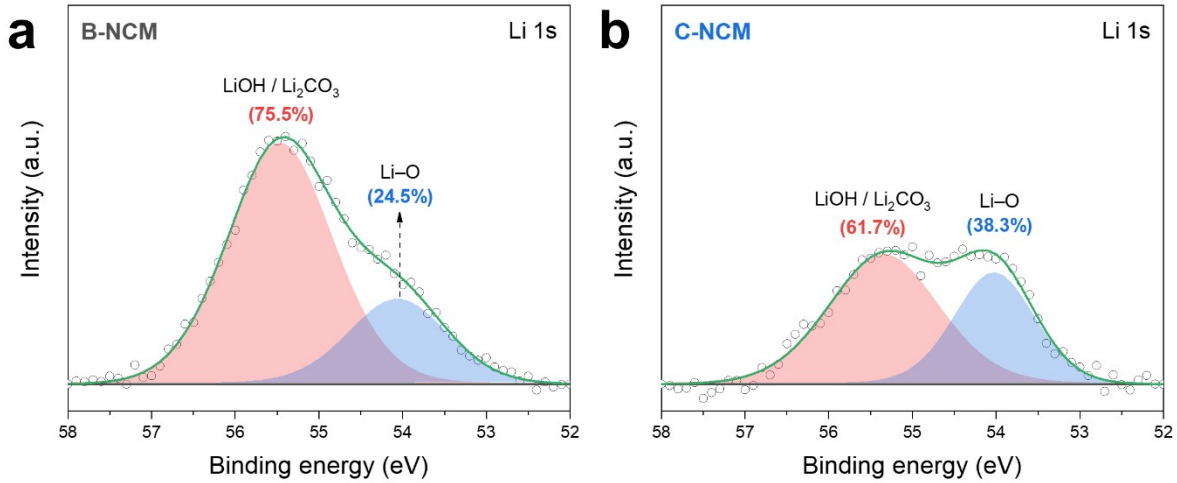

Fig. S9 Li 1s XPS spectra collected from the surface of pristine (a) B-NCM and (b) C-NCM cathodes (surface-sensitive mode, probing depth ≤ 10 nm).

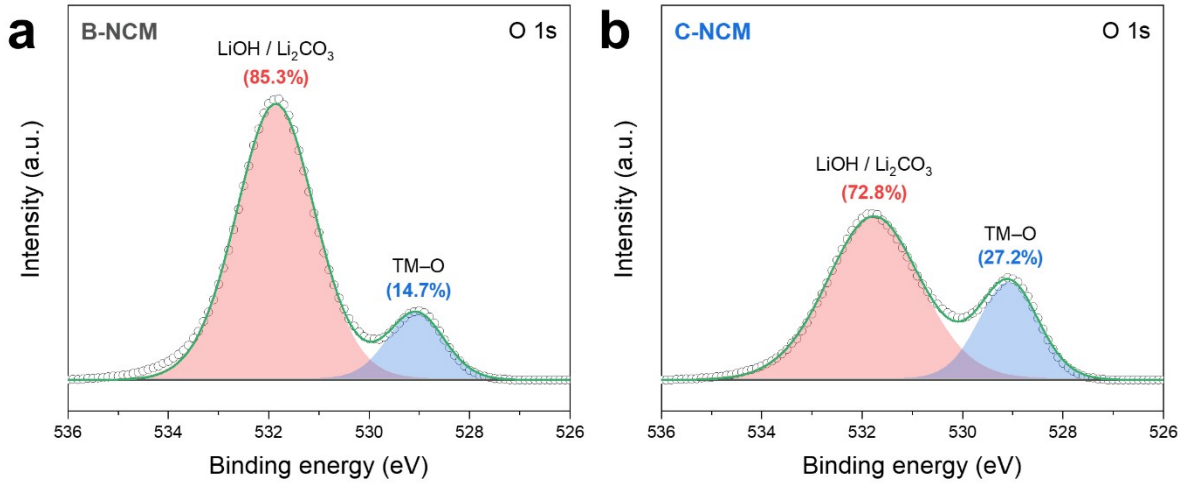

Fig. S10 O 1s XPS spectra collected from the surface of pristine (a) B-NCM and (b) C-NCM cathodes (surface-sensitive mode, probing depth ≤ 10 nm).

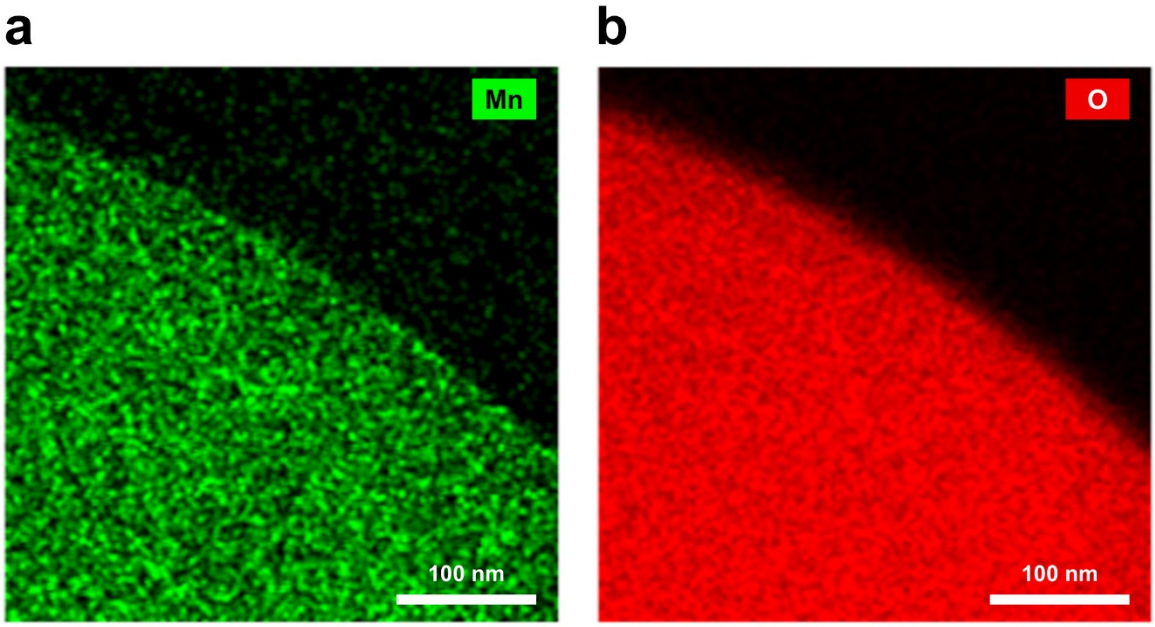

Fig. S11 TEM-EDS elemental maps of (a) Mn and (b) O in B-NCM cathode.

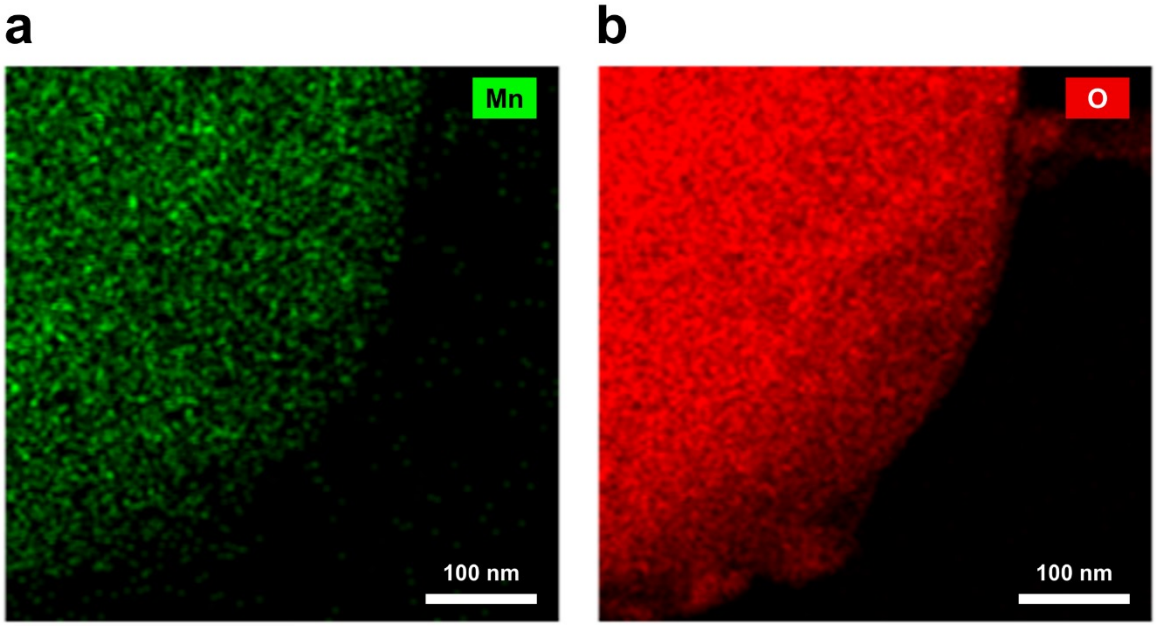

Fig. S12 TEM-EDS elemental maps of (a) Mn and (b) O in I-NCM cathode.

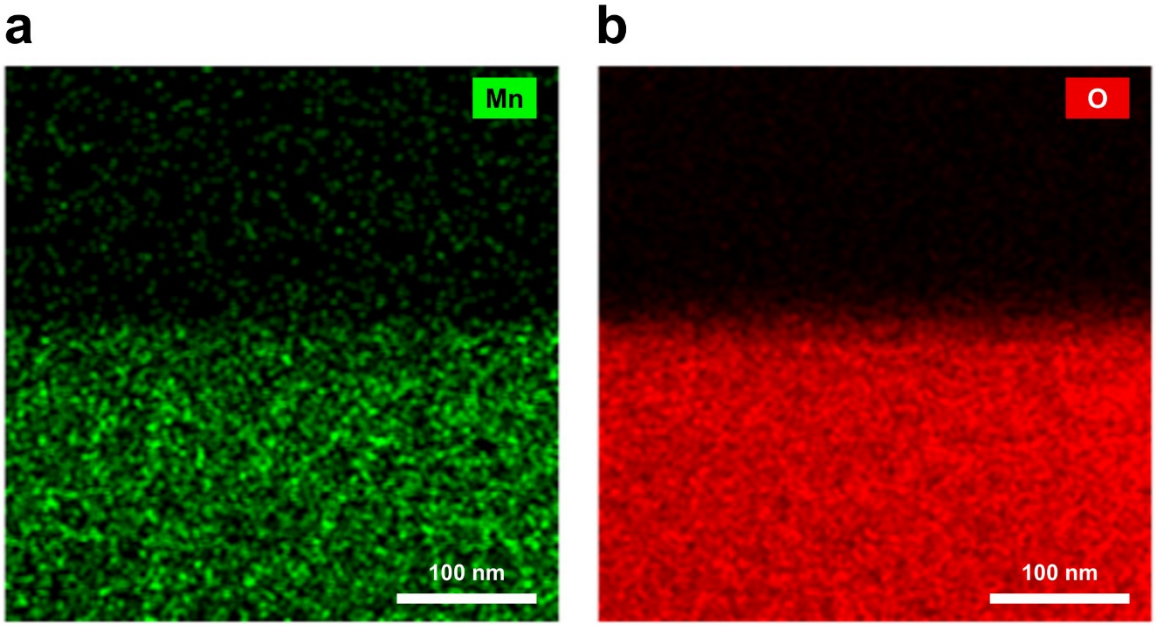

Fig. S13 TEM-EDS elemental maps of (a) Mn and (b) O in C-NCM cathode.

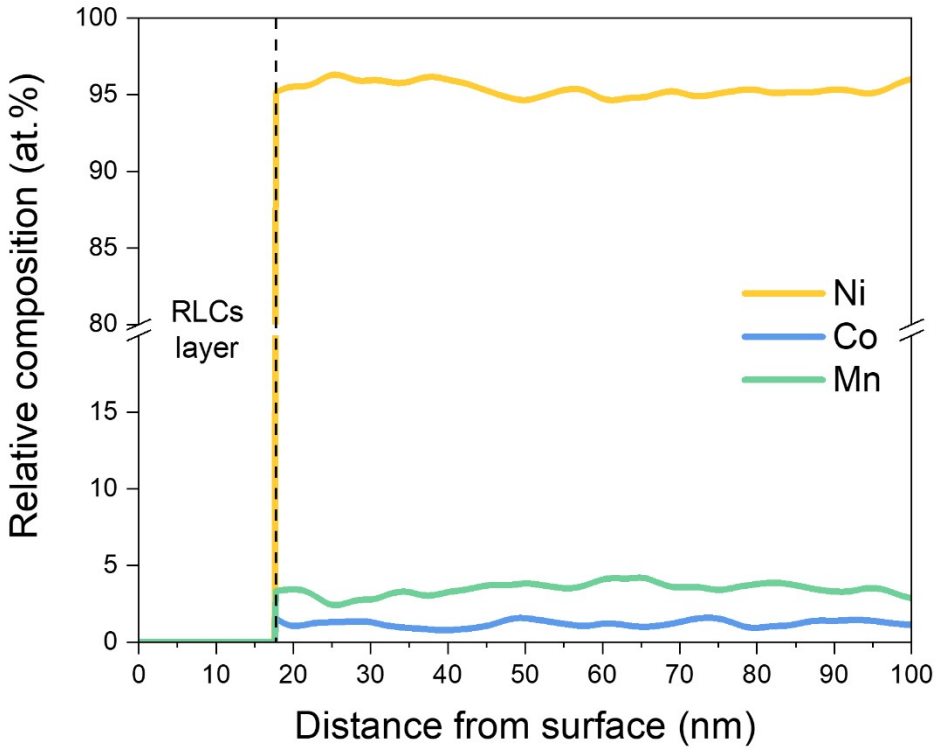

Fig. S14 TEM-EDS line scan profile of I-NCM cathode along the residual lithium compounds (RLCs) layer direction (indicated by the yellow arrow in Fig. 3b).

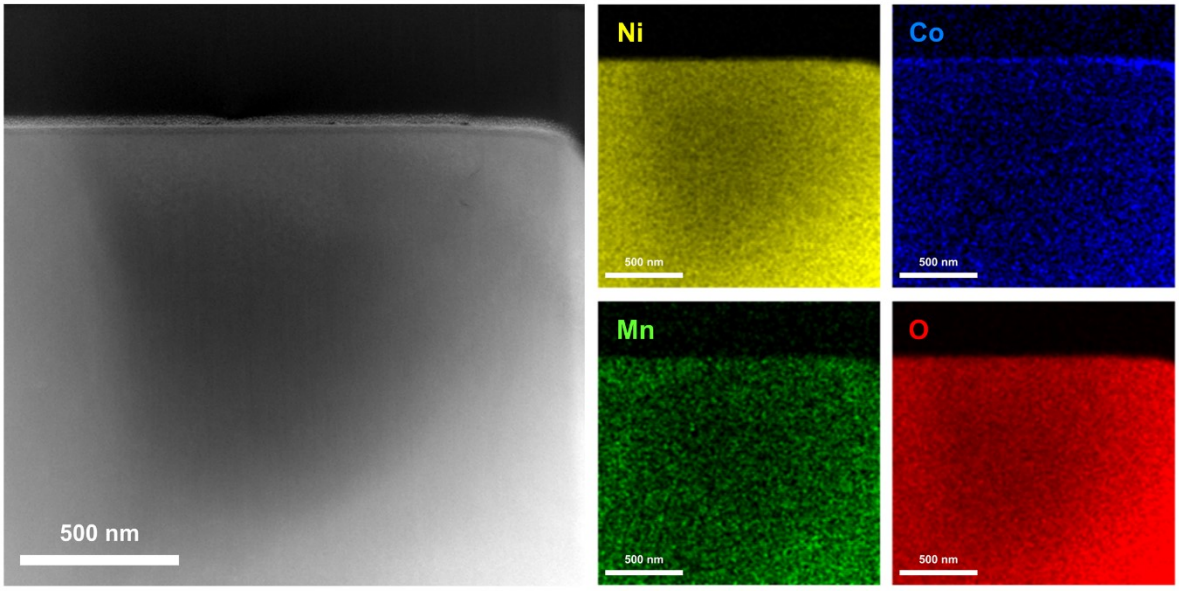

Fig. S15 Low magnification (120kX) TEM image and corresponding EDS elemental maps of C-NCM cathode.

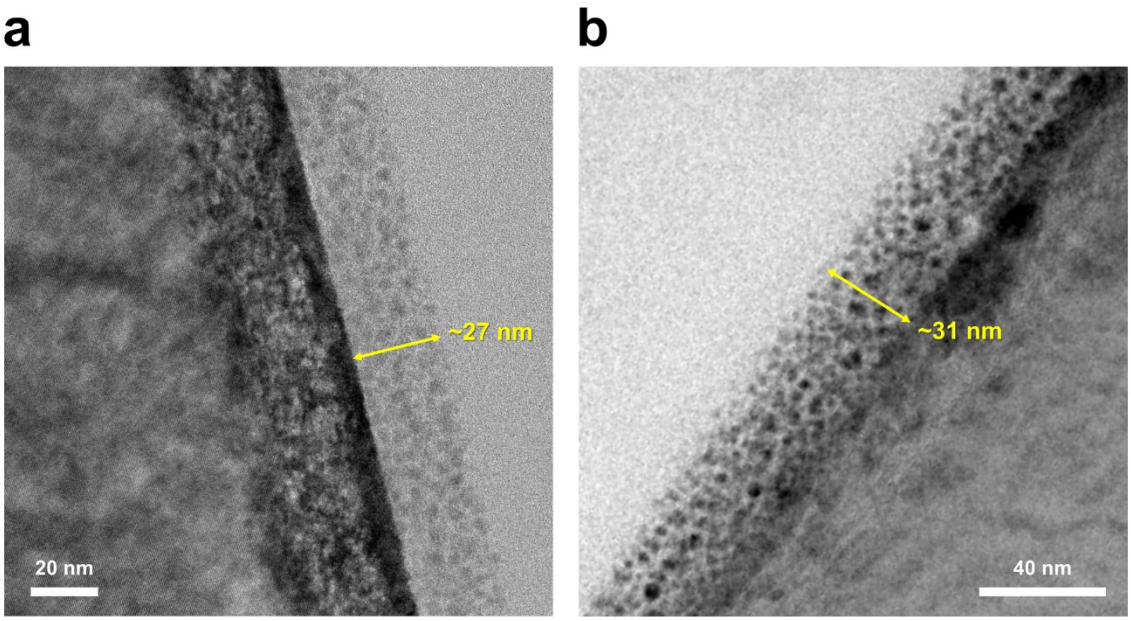

Fig. S16 Additional TEM images of C-NCM cathode: (a) 150kX and (b) 600kX. The TEM images shown in Fig. 3c, Fig. S16a, and Fig. S16b were obtained from different particles for comparison of the coating layer thickness across particles. The thickness of the coating layer is indicated by yellow arrows, and the corresponding thickness values are summarized in Table S6, which includes the mean and standard deviation (s.d.).

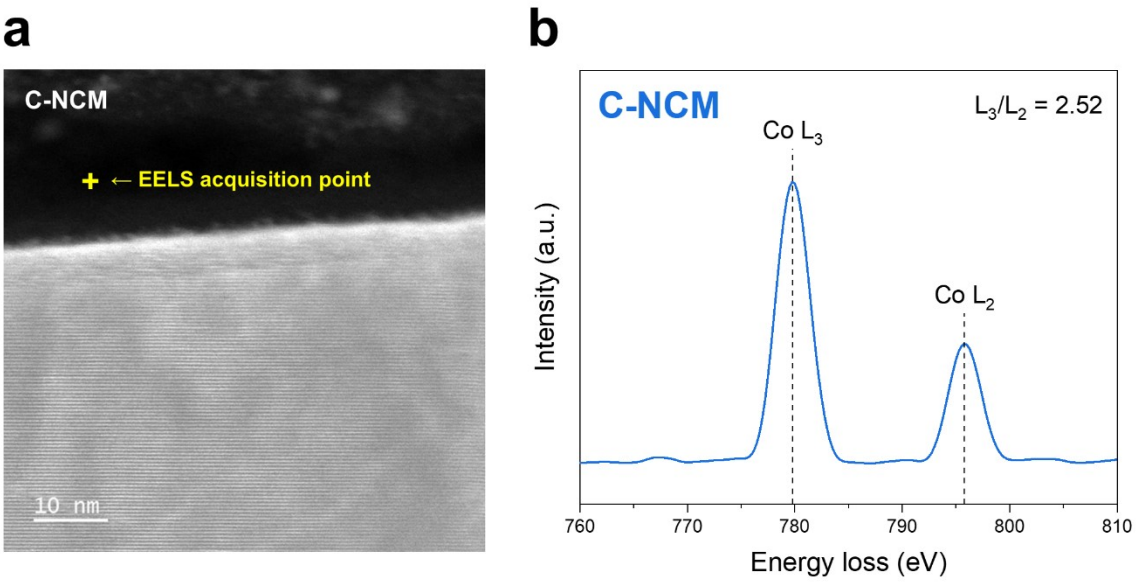

Fig. S17 (a) STEM image of pristine C-NCM cathode. (b) Corresponding Co L-edge EELS spectrum acquired from the amorphous Co-rich coating layer (at the position indicated by the yellow cross in Fig. S17a).

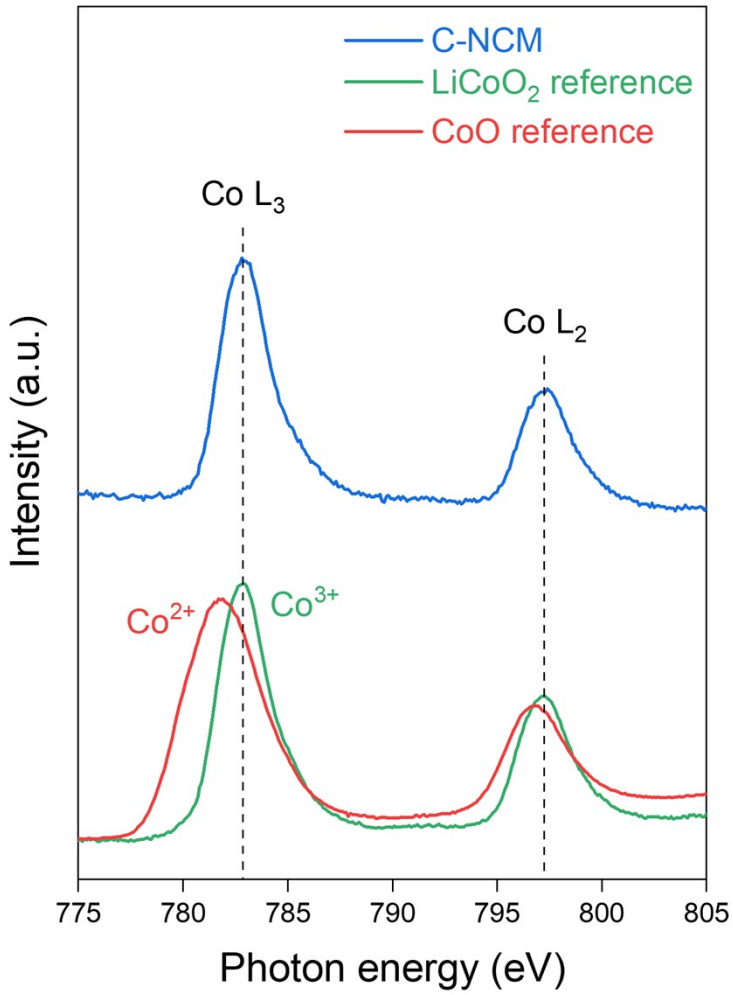

Fig. S18 Co L-edge soft XAS spectra of pristine C-NCM cathode, compared with reference $LiCoO_2$ and CoO samples (TEY mode, probing depth ≤ 10 nm, spectral resolution = 0.1 eV).

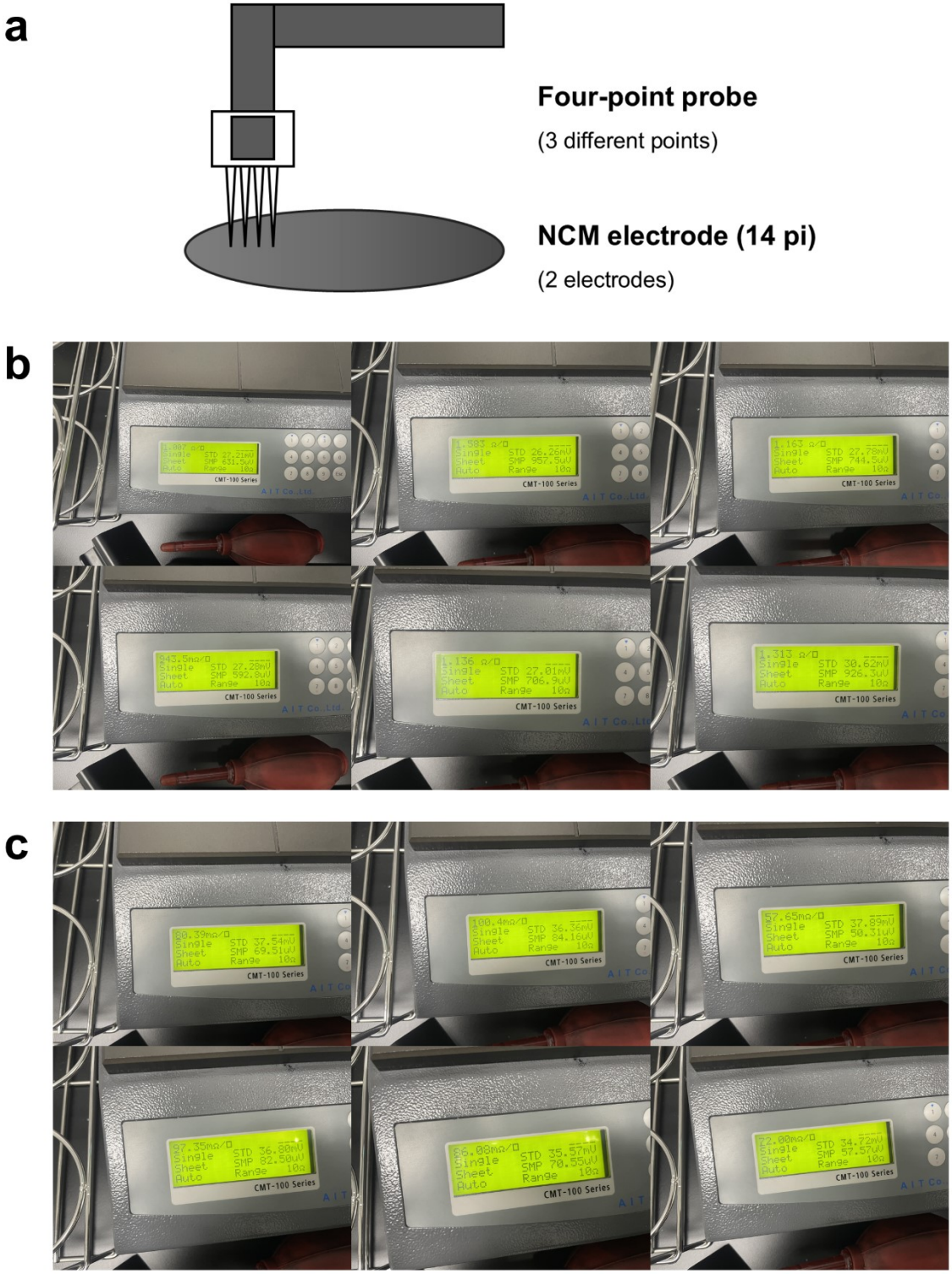

Fig. S19 (a) Schematic illustration of the four-point probe resistivity measurement for NCM electrodes. Measurements were conducted on two independently prepared electrodes per sample, with three repeated measurements on each electrode (n = 6). Optical photographs of the four-point probe resistivity measurement screens for (b) B-NCM and (c) C-NCM electrodes.

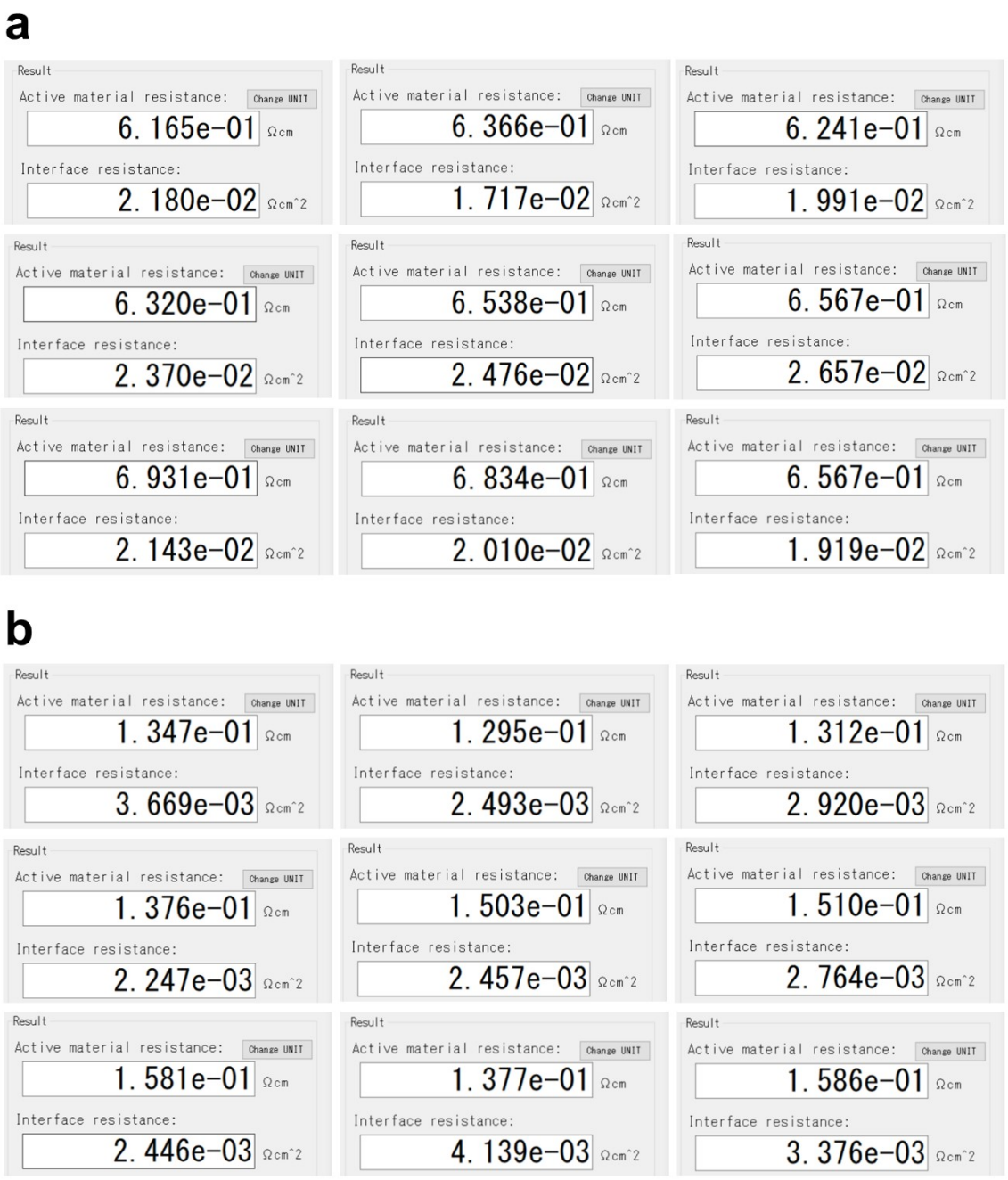

Fig. S20 Screenshots of the electrode resistance measurements for (a) B-NCM and (b) C-NCM electrodes. The "Active material resistance (Ω·cm)" corresponds to the composite resistance (NCM + Super P + PVdF), while the "Interface resistance ($\Omega \cdot cm^2$)" represents the contact resistance between the composite electrode and the Al current collector. Measurements were conducted on three independently prepared electrodes per sample, with three repeated measurements on each electrode (n = 9).

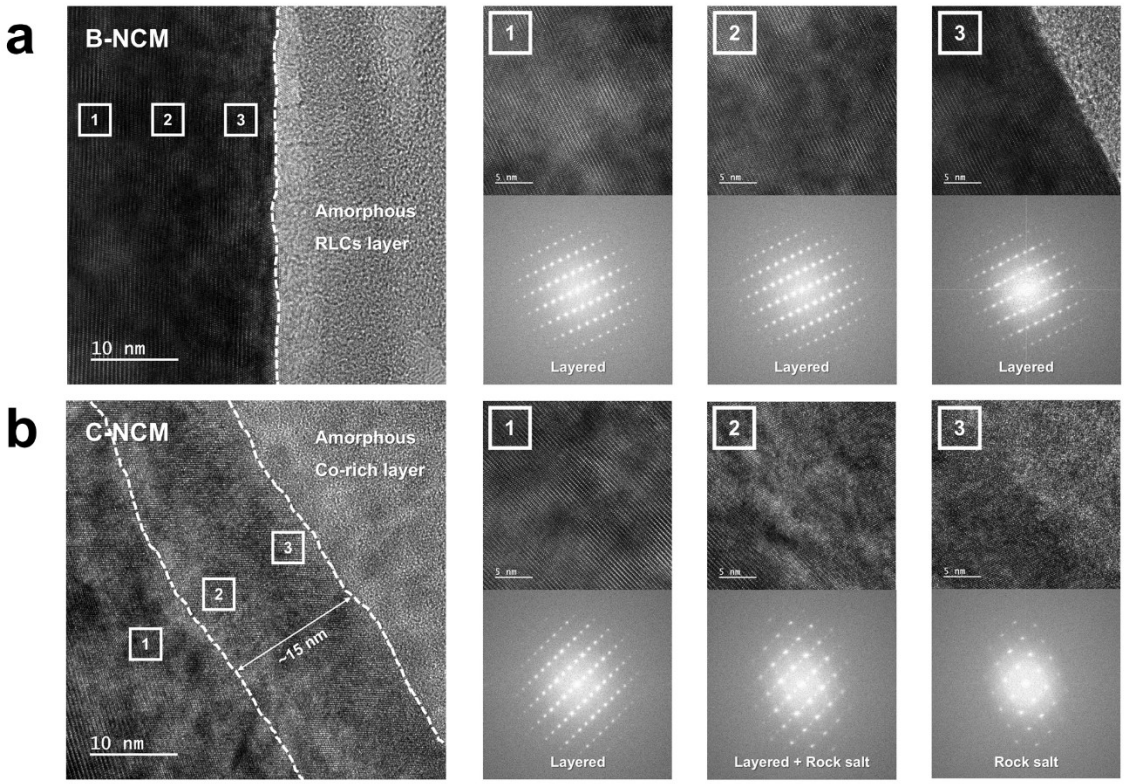

Fig. S21 HRTEM images and corresponding fast Fourier transform (FFT) patterns of pristine (a) B-NCM and (b) C-NCM cathodes. The FFT pattern acquisition points are indicated by white numbered labels (1–3) in the corresponding HRTEM images.

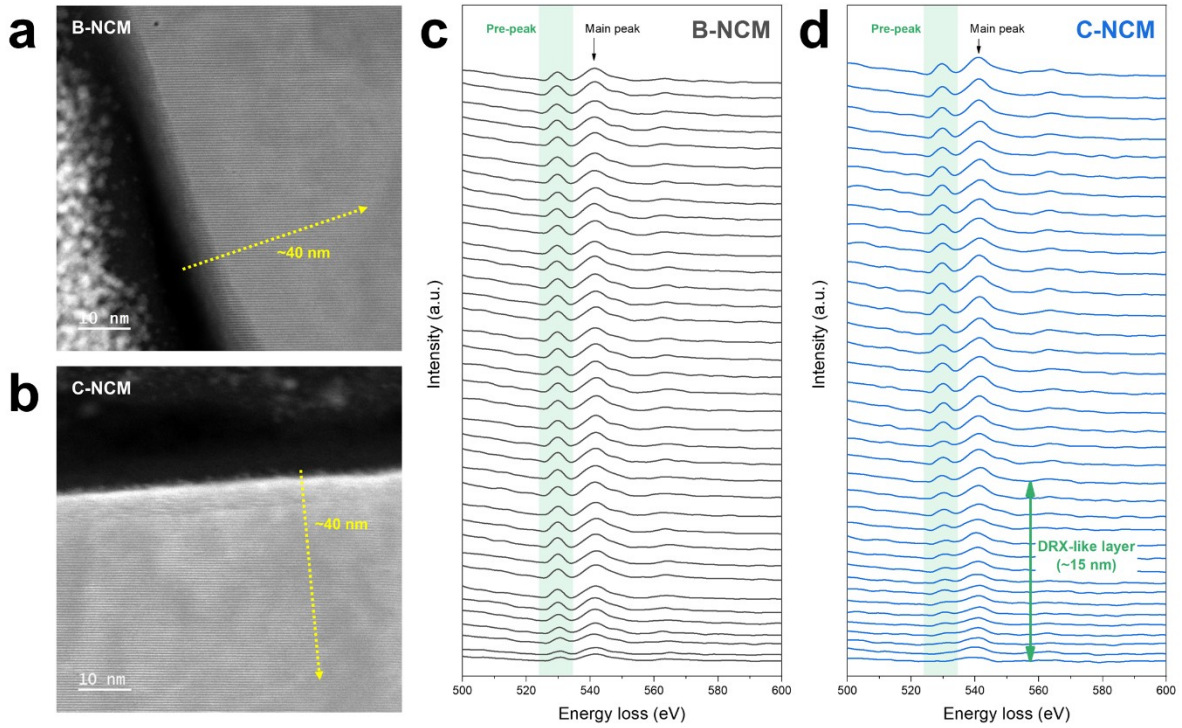

Fig. S22 STEM images of pristine (a) B-NCM and (b) C-NCM cathodes. Corresponding O K-edge EELS spectra of (c) B-NCM and (d) C-NCM cathodes, collected from the surface to the bulk (along the yellow arrow, indicating the scanning direction). The oxygen pre-peak region is highlighted by a green shaded area.

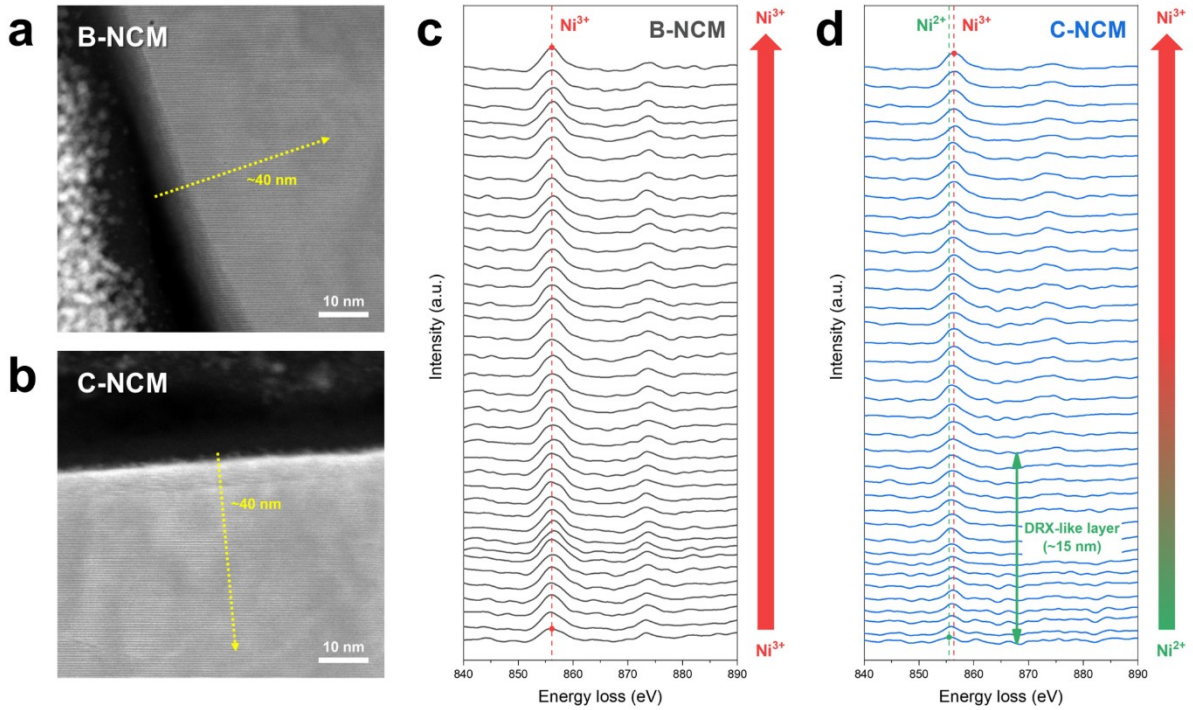

Fig. S23 STEM images of pristine (a) B-NCM and (b) C-NCM cathodes. Corresponding Ni L-edge EELS spectra of (c) B-NCM and (d) C-NCM cathodes, collected from the surface to the bulk (along the yellow arrow, indicating the scanning direction). Reference lines for Ni^{2+} and Ni^{3+} at the Ni L_3-edge are indicated by green and red dashed lines, respectively.

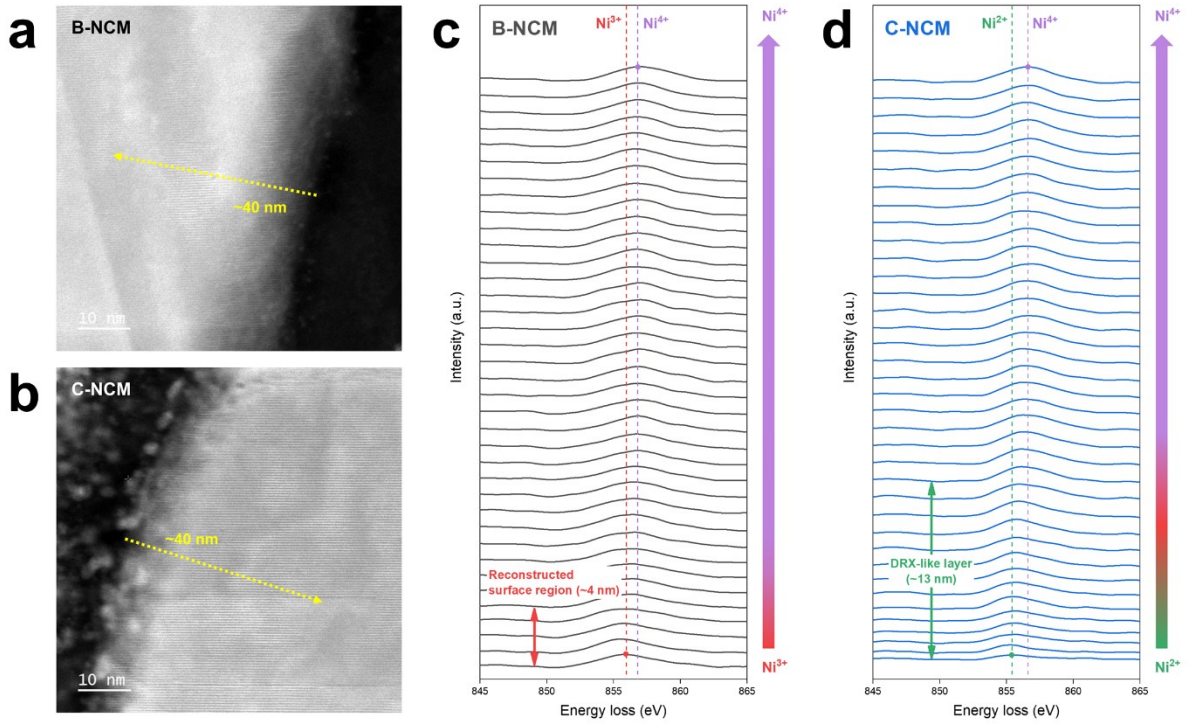

Fig. S24 STEM images of (a) B-NCM and (b) C-NCM cathodes at the charged state of 4.3 V. Corresponding Ni L-edge EELS spectra of (c) B-NCM and (d) C-NCM cathodes, collected from the surface to the bulk (along the yellow arrow, indicating the scanning direction). Reference lines for Ni^{2+}, Ni^{3+}, and Ni^{4+} at the Ni L_3-edge are indicated by green, red, and purple dashed lines, respectively.

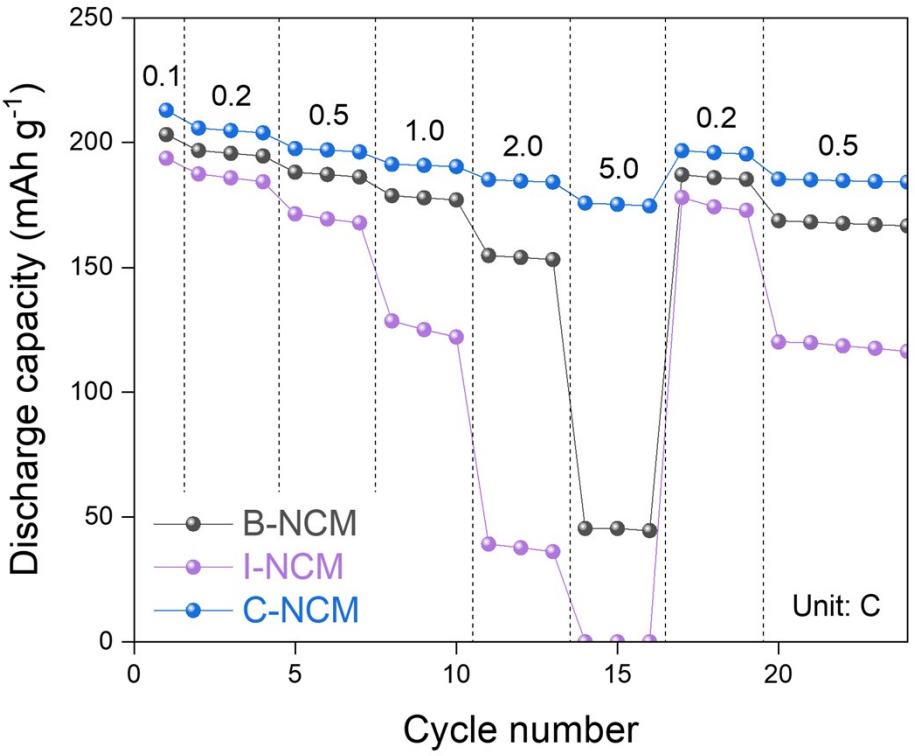

Fig. S25 Comparison of discharge rate capabilities of B-NCM, I-NCM, and C-NCM cathodes. All tests were conducted at 25 °C within a voltage window of 3.0–4.3 V.

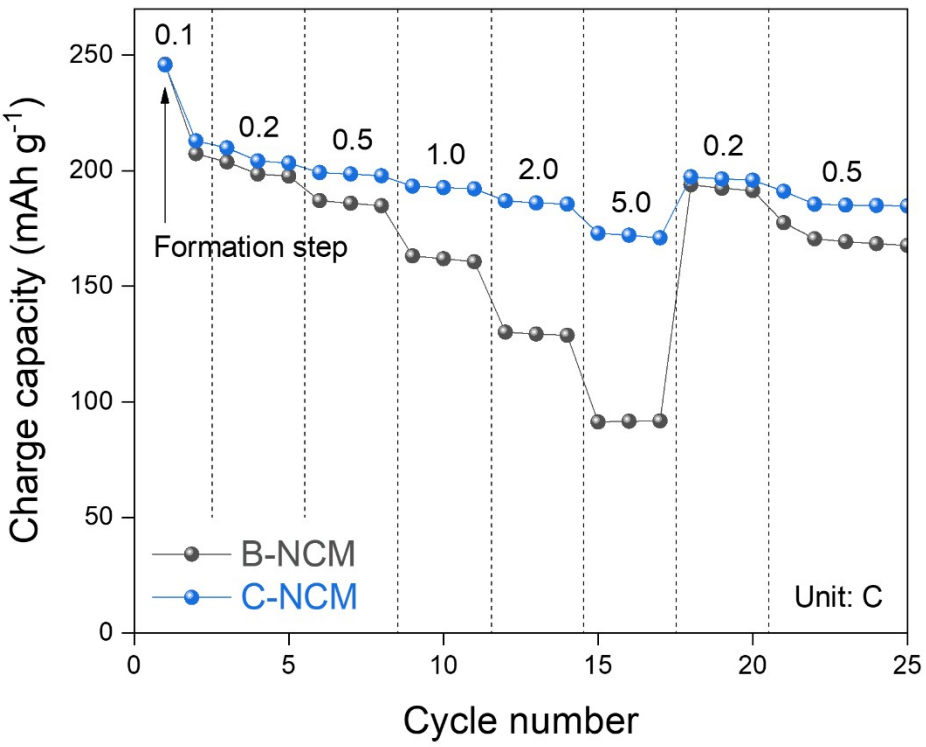

Fig. S26 Charge rate capabilities of B-NCM and C-NCM cathodes using a constant current–constant voltage (CC–CV) charging mode. All tests were conducted at 25 °C within a voltage window of 3.0–4.3 V.

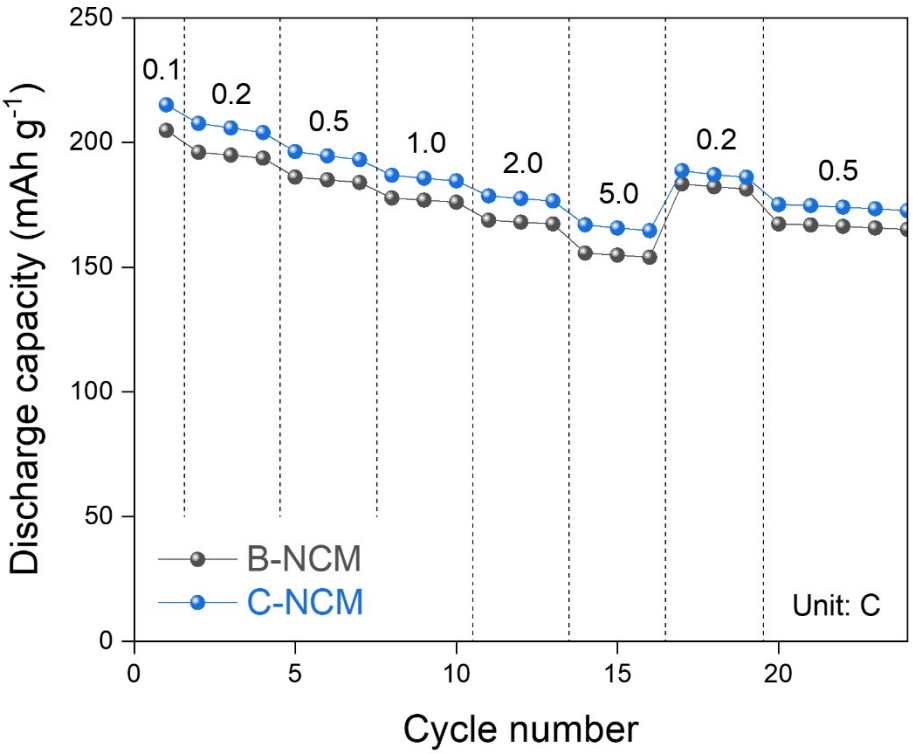

Fig. S27 Discharge rate capabilities of B-NCM and C-NCM cathodes measured using a conductive electrode composition of 80:10:10 (NCM : Super P : PVdF, wt.%) to minimize electronic transport limitations. All tests were conducted at 25 °C within a voltage window of 3.0–4.3 V.

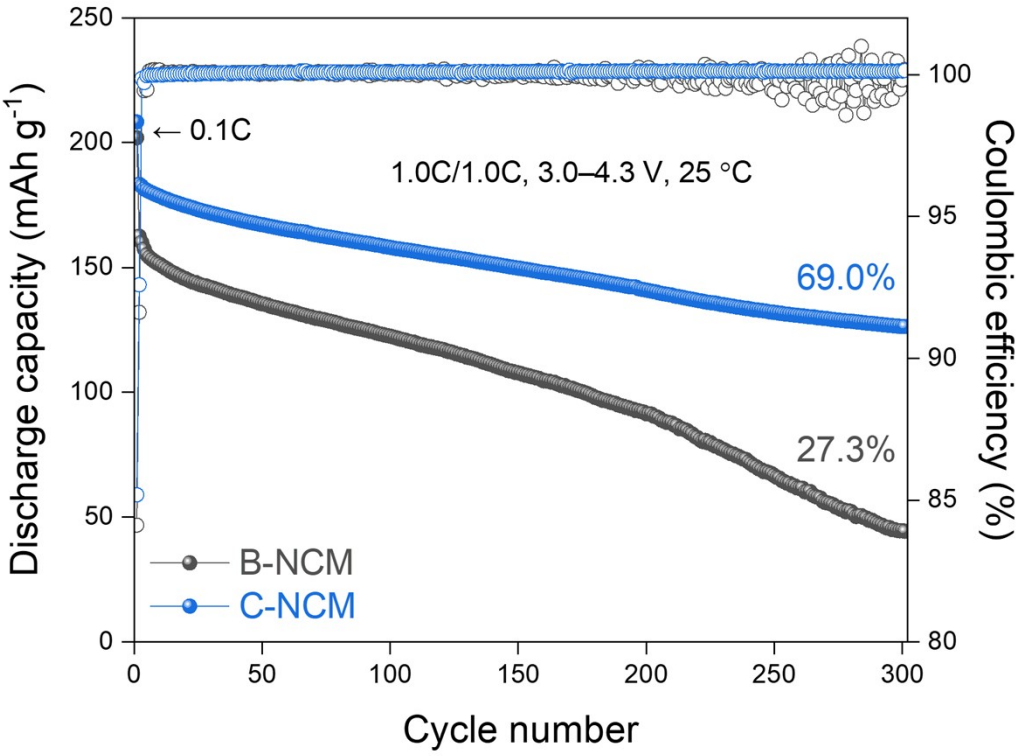

Fig. S28 Long-term cycling performance of B-NCM and C-NCM cathodes over 300 cycles. All tests were conducted at 25 °C within a voltage window of 3.0–4.3 V.

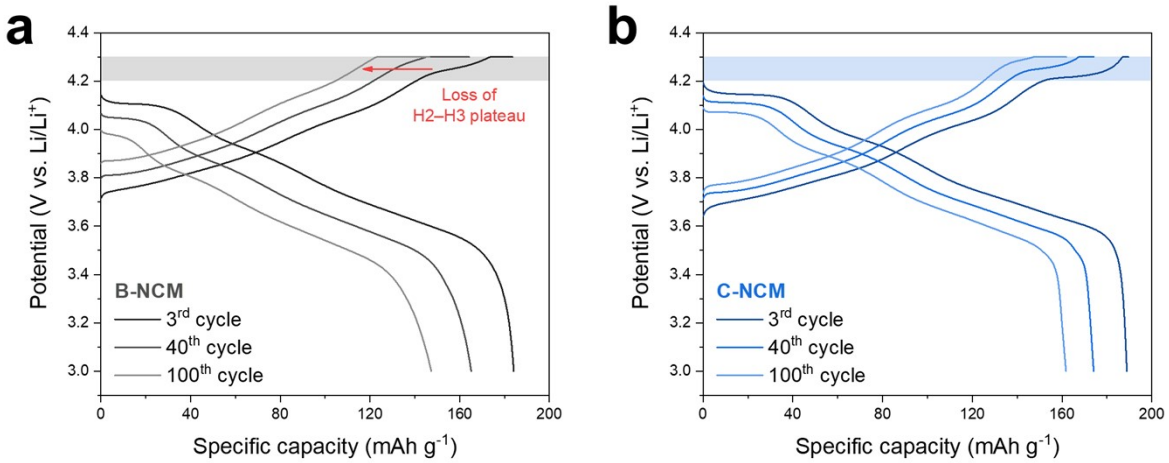

Fig. S29 Voltage profiles of (a) B-NCM and (b) C-NCM cathodes measured at 0.5 C for the 3rd, 40th, and 100th cycles, corresponding to the differential capacity (dQ/dV) curves shown in Fig. 4g–h. The shaded region (4.2–4.3 V) highlights the H2–H3 plateau.

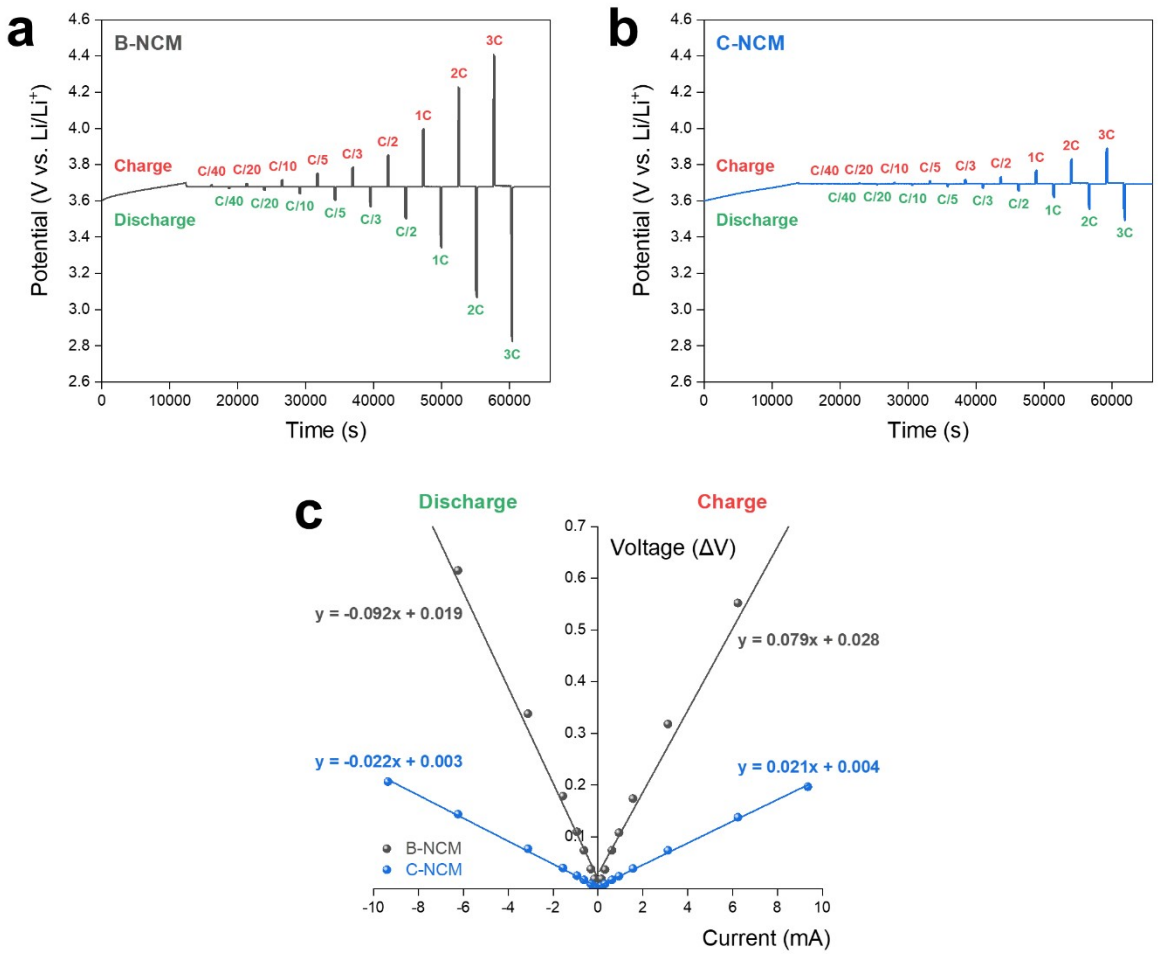

Fig. S30 Voltage responses of (a) B-NCM and (b) C-NCM cathodes during DC-IR experiments at 25 °C. (c) Plots of the change in voltage vs. current of B-NCM and C-NCM cathodes, with linear fits.

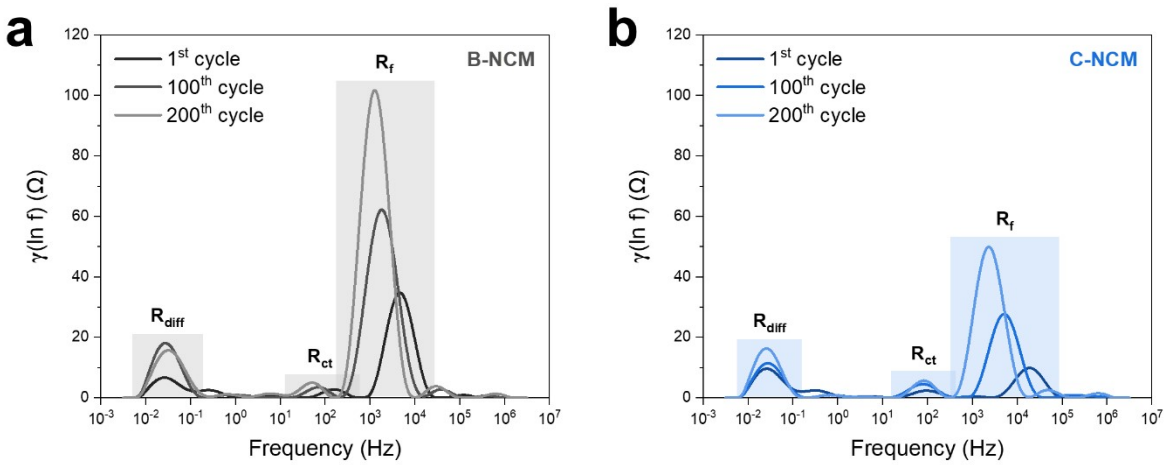

Fig. S31 Distribution of relaxation times (DRT) profiles obtained from the original EIS data of (a) B-NCM and (b) C-NCM cathodes at selected cycles.

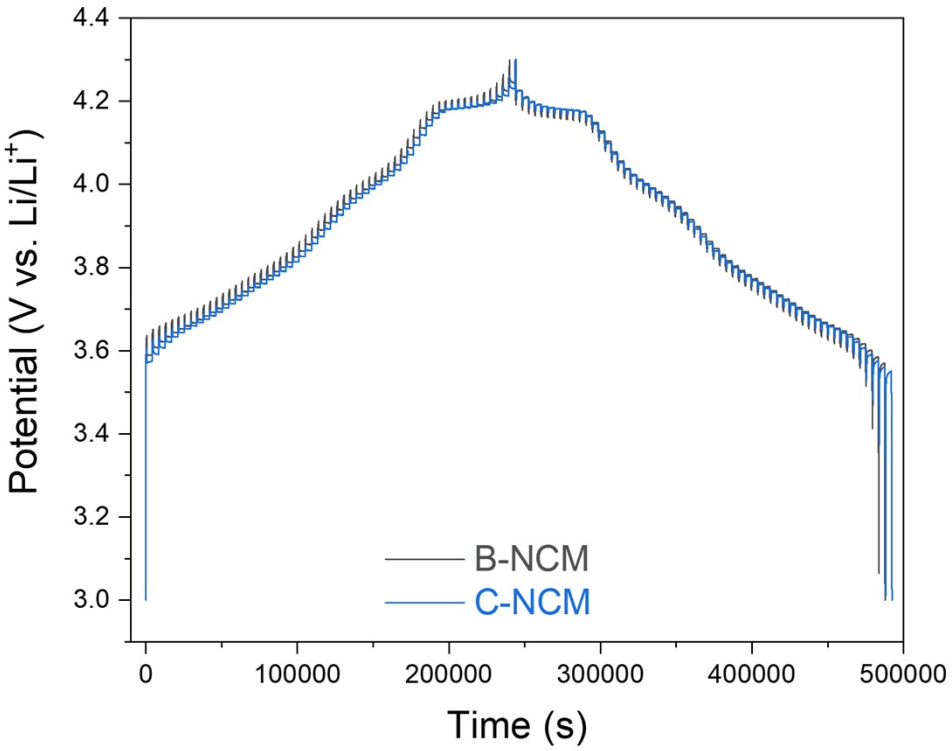

Fig. S32 GITT curves of B-NCM and C-NCM cathodes (3.0–4.3 V, 0.1 C pulse for 10 min, 1 h relaxation, 25 °C).

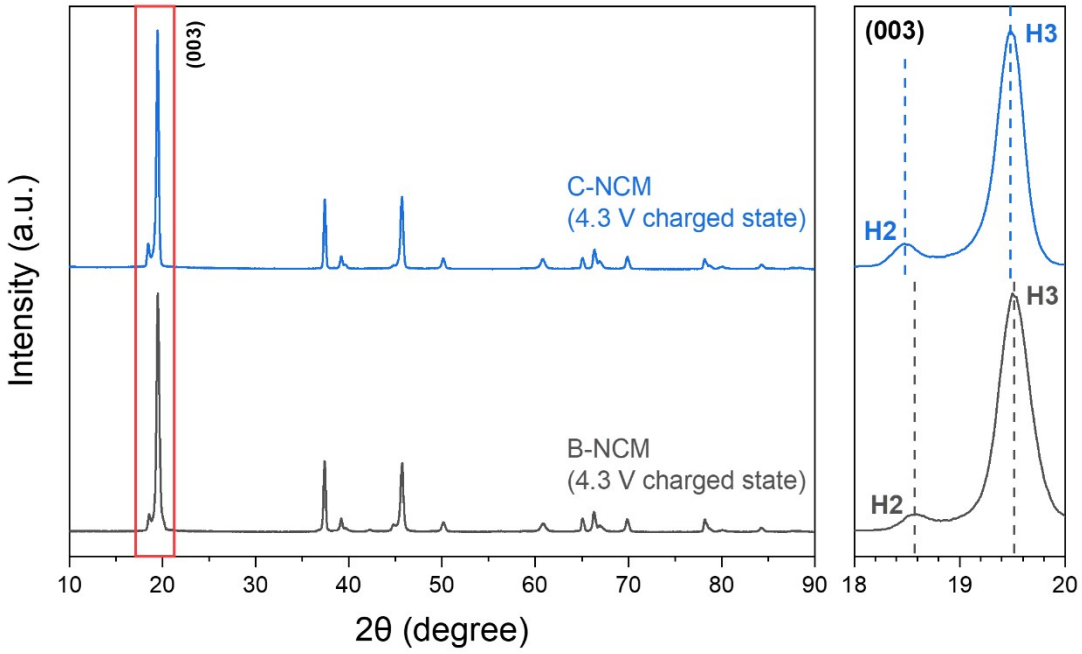

Fig. S33 HRXRD patterns of B-NCM and C-NCM cathodes at the charged state of 4.3 V, with locally enlarged views (Cu Kα radiation, λ = 1.5406 Å).

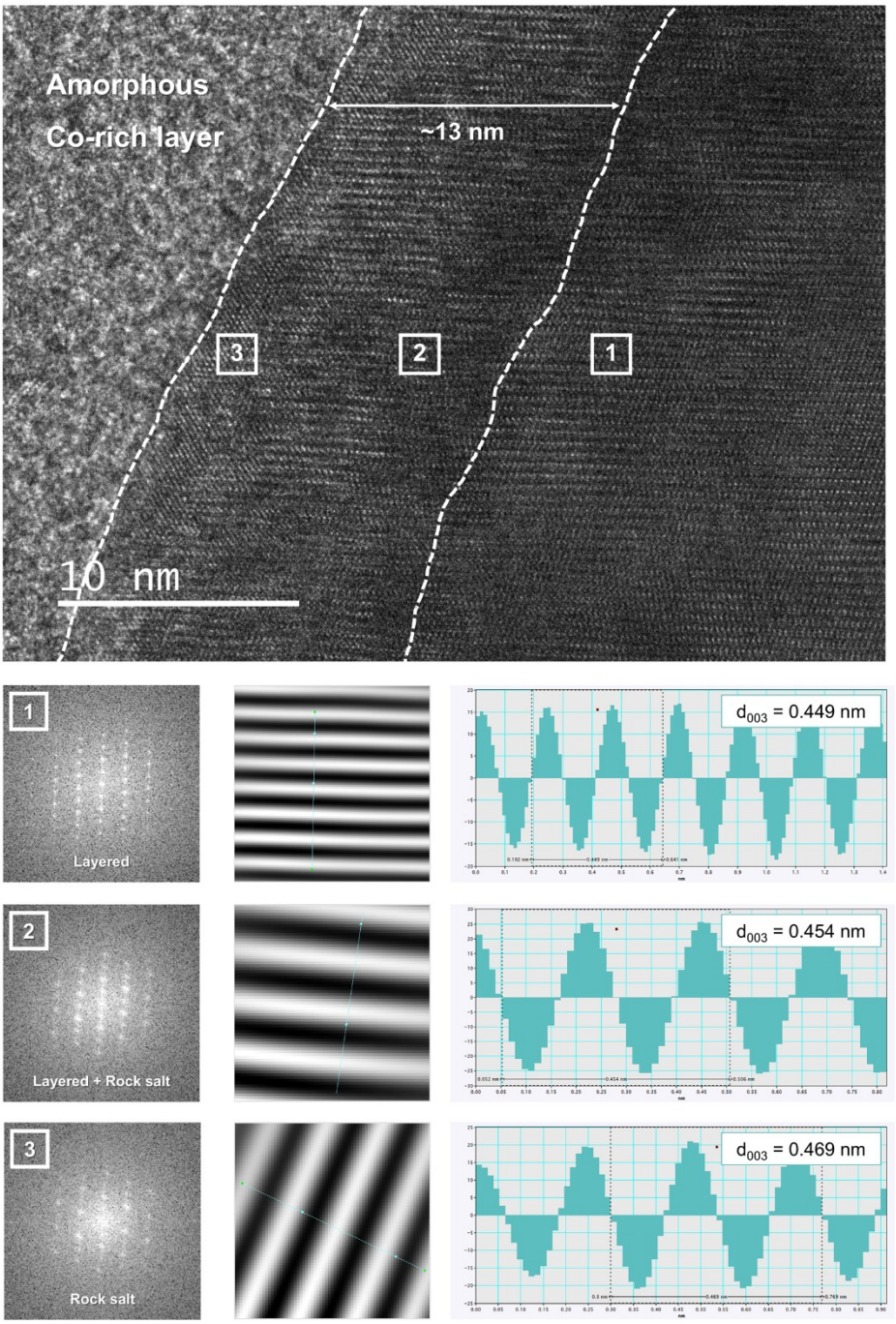

Fig. S34 HRTEM image of C-NCM cathode at the charged state of 4.3 V, along with the corresponding fast Fourier transform (FFT), inverse FFT (IFFT) patterns, and line profile images. The FFT pattern acquisition points are indicated by white numbered labels (1–3) in the corresponding HRTEM image.

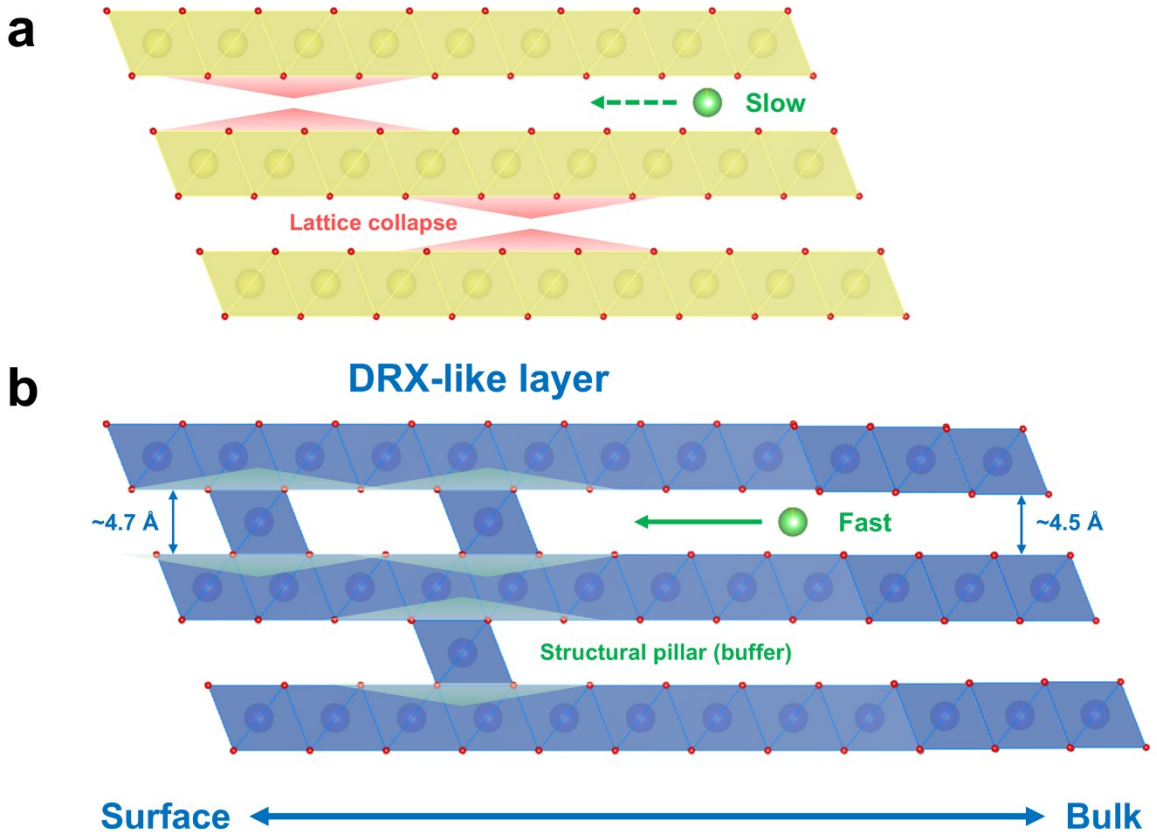

Fig. S35 Schematic illustrations of (a) conventional layered oxide cathodes (e.g., B-NCM) and (b) C-NCM cathodes in their highly delithiated state (high-voltage region).

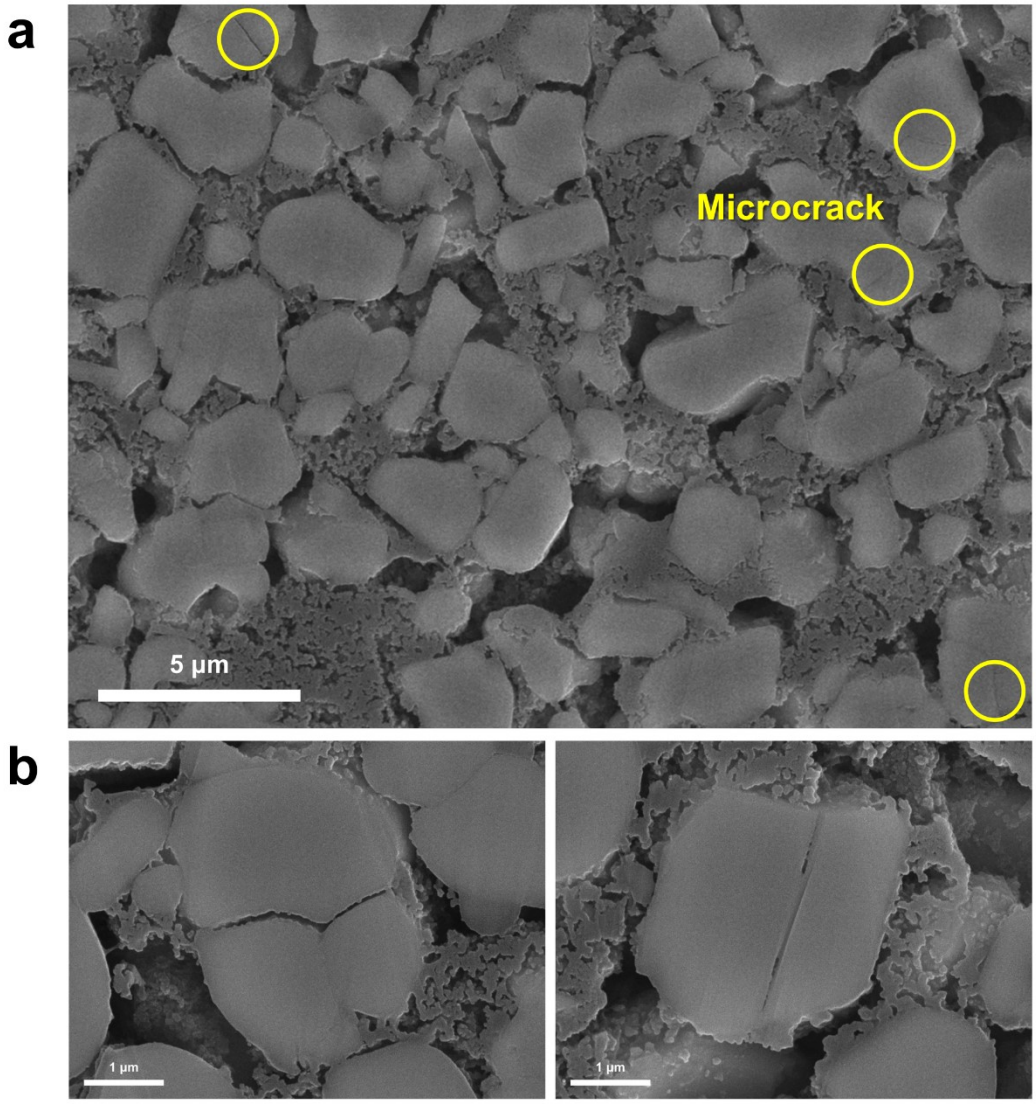

Fig. S36 Cross-sectional SEM images of B-NCM cathode after 200 cycles at (a) low magnification (×5,000) and (b) high magnification (×20,000).

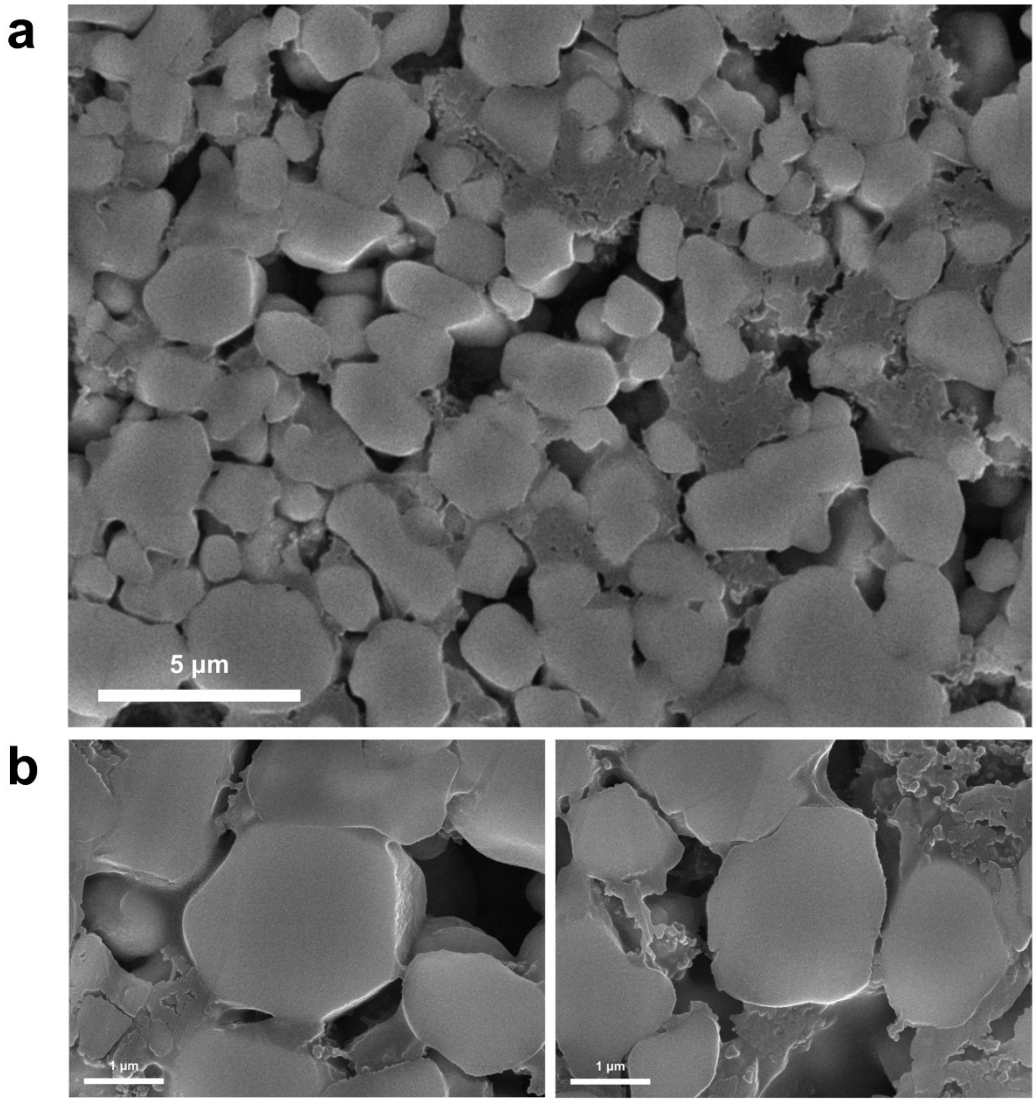

Fig. S37 Cross-sectional SEM images of C-NCM cathode after 200 cycles at (a) low magnification (×5,000) and (b) high magnification (×20,000).

Fig. S38 Optical photograph of pouch-type half cells with B-NCM and C-NCM cathodes (areal capacity = 2 mAh cm^{-2}, cathode area = 6 cm × 3 cm = 18 cm^2, cell capacity = 36 mAh) with a ruler for scale.

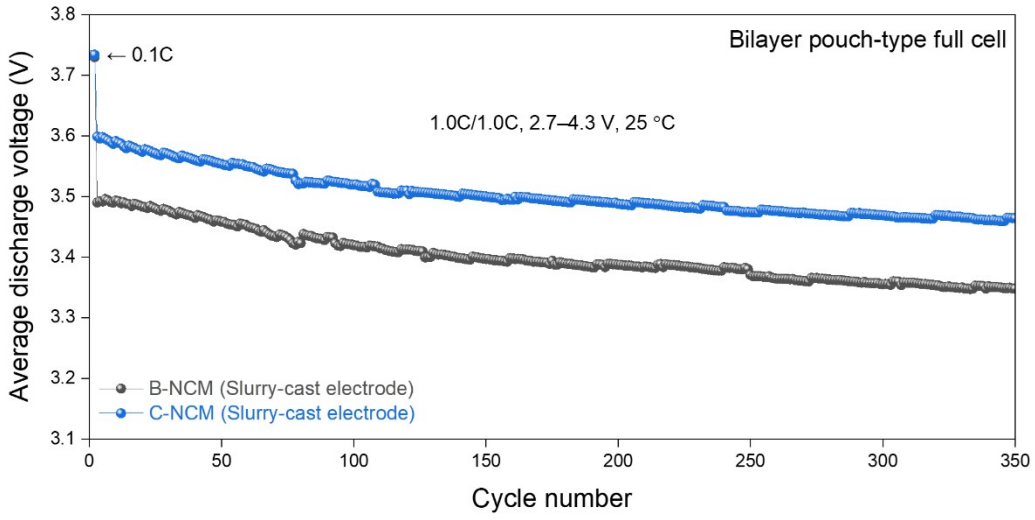

Fig. S39 Average discharge voltage evolution (1.0/1.0 C) of B-NCM and C-NCM cathodes in bilayer pouch-type full cells with slurry-cast NCM electrodes (~4.1 mAh cm^{-2}). All tests were conducted at 25 °C within a voltage window of 2.7–4.3 V.

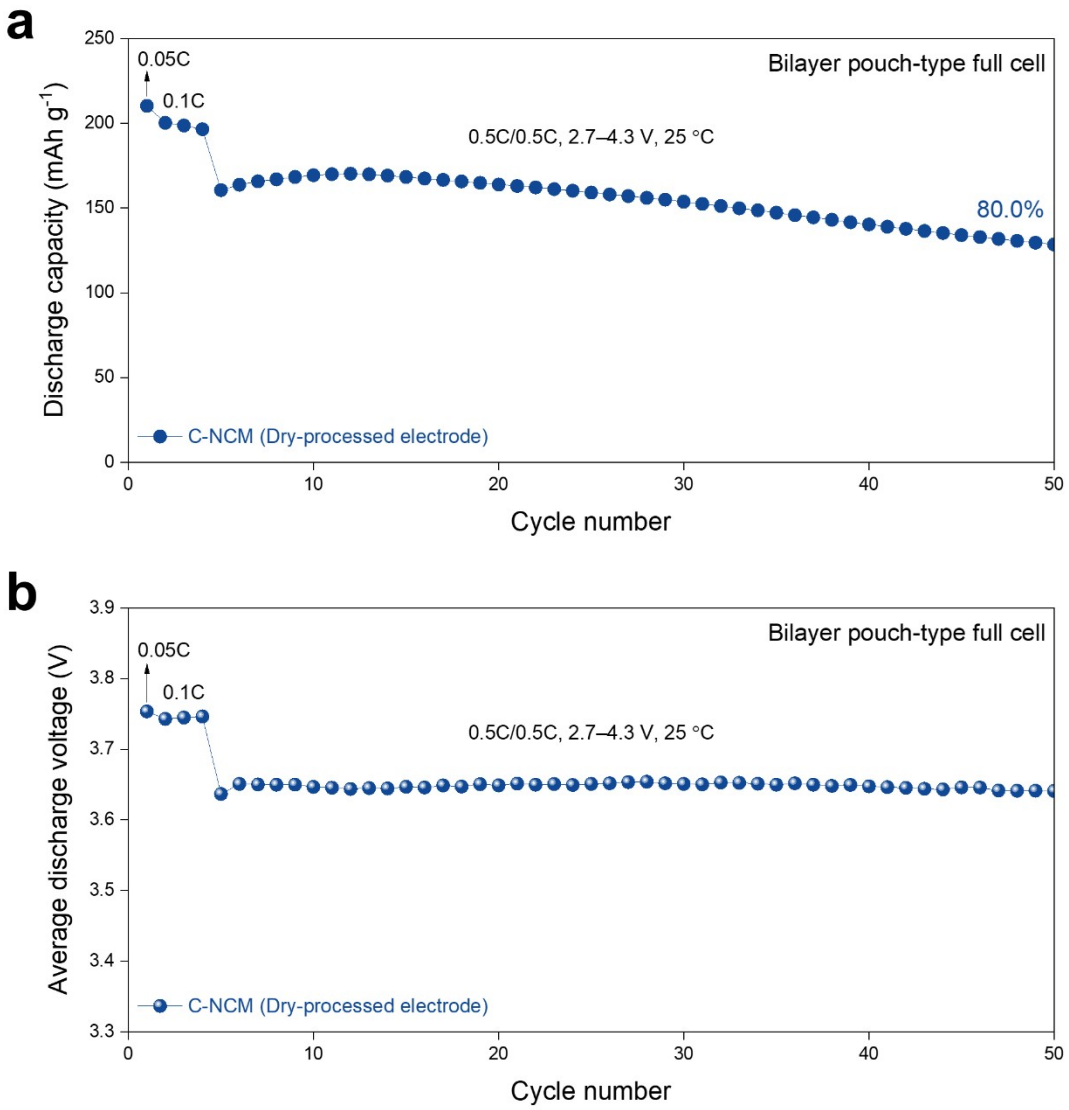

Fig. S40 (a) Cycling performance (specific discharge capacity, mAh g^{-1}) and (b) average discharge voltage evolution (0.5/0.5 C) of C-NCM cathode in a bilayer pouch-type full cell with a high-loading dry-processed NCM electrode (~8.1 mAh cm^{-2}). All tests were conducted at 25 °C within a voltage window of 2.7–4.3 V.

Table S4 ICP-OES results of pristine B-NCM and C-NCM cathode.

Sample	Li / (Ni+Co+Mn)	Ni / (Ni+Co+Mn)	Co / (Ni+Co+Mn)	Mn / (Ni+Co+Mn)
B-NCM	1.016	0.957	0.008	0.035
C-NCM	1.001	0.950	0.018	0.032

Table S5 Rietveld refinement results obtained from HRXRD pattern of C-NCM cathode.

Atom	Site	z	Occupancy	Uiso ($Å^2$)
Li1	3b	0.00000	0.9815	0.00189
Ni1	3b	0.00000	0.0185	0.00189
Ni2	3a	0.50000	0.9415	0.00095
Co	3a	0.50000	0.0180	0.00095
Mn	3a	0.50000	0.0320	0.00095
Li2	3a	0.50000	0.0185	0.00095
O	6c	0.24065	1.0000	0.00362

Refined cell parameters: a = b = 2.87707 Å, c = 14.19522 Å, V = 101.759 $Å^3$

Li^+/Ni^{2+} cation mixing = 1.85%

R_{wp} = 13.498%

Reduced χ^2 = 5.11

Table S6 Coating layer thickness measured from the TEM images of C-NCM cathode, obtained from different particles (Fig. 3c, Fig. S16a, and Fig. S16b). The mean and standard deviation (s.d.) were calculated from all three measurements.

Sample	Particle ID	Image reference	Coating layer thickness (nm)	Mean ± s.d. (nm)
C-NCM	#1	Fig. 3c	~28	28.67 ± 2.08
	#2	Fig. S16a	~27	
	#3	Fig. S16b	~31	

Table S7 Comparison of dry coating characteristics reported in previous studies and this work. NPs denotes nanoparticles and is used only when the coating material was explicitly described as nanoparticulate in the corresponding references. The cited references can be found in the reference list of the main manuscript.

Work	Cathode active material	Coating material	Coating content	Coating morphology	Gradient structure
This work	$LiNi_{0.96}Co_{0.01}Mn_{0.03}O_2$ (single-crystal)	Co_3O_4 NPs (~100 nm)	1.0 wt.%	Thin, uniform (~30 nm)	Concentration–structure dual-gradient
Ref [25]	$LiNi_{0.8}Co_{0.1}Mn_{0.1}O_2$ (polycrystalline)	$Al(OH)_3$ NPs	1.0 wt.%	Island-type	Not reported
Ref [51]	$LiNi_{0.91}Co_{0.06}Mn_{0.03}O_2$ (polycrystalline)	$Al(OH)_3$, $Co(OH)_2$	0.04 molar equivalents	Island-type	Concentration gradient
Ref [79]	$LiNi_{0.70}Co_{0.15}Mn_{0.15}O_2$ (polycrystalline)	Al_2O_3 NPs	1.0 wt.%	Island-type	Not reported
Ref [26]	$LiNi_{0.70}Co_{0.15}Mn_{0.15}O_2$ (polycrystalline)	Al_2O_3 NPs (~12 nm)	1.0 wt.%	Inhomogeneous	Not reported
Ref [27]	$LiNi_{0.70}Co_{0.15}Mn_{0.15}O_2$ (polycrystalline)	Al_2O_3, ZrO_2, TiO_2 NPs	1.0 wt.%	Island-type	Not reported
Ref [28]	$LiNi_{0.6}Co_{0.2}Mn_{0.2}O_2$ (polycrystalline)	$Mn_3(PO_4)_2$	1.0 wt.%	Island-type	Not reported
Ref [29]	$LiNi_{0.8}Co_{0.1}Mn_{0.1}O_2$ (polycrystalline)	$Co(OH)_2$ NPs	4.0 wt.%	Island-type	Not reported
Ref [30]	$LiNi_{0.91}Co_{0.06}Mn_{0.03}O_2$ (polycrystalline)	$Co(OH)_2$	4.0 wt.%	Island-type	Concentration gradient
Ref [31]	$LiNi_{0.91}Co_{0.06}Mn_{0.03}O_2$ (polycrystalline)	Co_3O_4 (< 1 μm)	1.0 wt.%	Island-type	Not reported

Table S8 Electrode parameters used for four-point probe resistivity and electrode resistance measurements.

Parameter	Value
Electrode composition (wt.%)	NCM : Super P : PVdF = 94 : 3 : 3
Electrode mass (g)	0.0241
Electrode area (cm^2, 14 mm-diameter disks)	1.539
Electrode thickness after calendering (μm)	54
Al current collector thickness (μm)	20
Electrode coating thickness (μm)	34
Areal mass loading (mg cm^{-2})	10.1
Electrode coating density (g cm^{-3})	3.0

Table S9 Four-point probe resistivity measurement results of B-NCM and C-NCM electrodes. Measurements were conducted on two independently prepared electrodes per sample, with three repeated measurements on each electrode (n = 6). The mean and standard deviation (s.d.) were calculated from all six measurements.

Sample	Electrode	Measurement ID	Sheet resistance (Ω sq^{-1})	Mean ± s.d. (Ω sq^{-1})
B-NCM	Electrode 1	#1-1	1.007	1.191 ± 0.231
		#1-2	1.583	
		#1-3	1.163	
	Electrode 2	#2-1	0.944	
		#2-2	1.136	
		#2-3	1.313	
C-NCM	Electrode 1	#1-1	0.097	0.082 ± 0.016
		#1-2	0.058	
		#1-3	0.080	
	Electrode 2	#2-1	0.072	
		#2-2	0.086	
		#2-3	0.100	

Table S10 Electrode resistance measurement results of B-NCM and C-NCM electrodes. Measurements were conducted on three independently prepared electrodes per sample, with three repeated measurements on each electrode (n = 9). The composite resistance (Ω·cm) and contact resistance (Ω·cm^2) were obtained from each measurement. The mean and standard deviation (s.d.) were calculated from all nine measurements.

Sample	Electrode	Measurement ID	Composite resistance (Ω·cm)	Contact resistance (Ω·cm^2)
B-NCM	Electrode 1	#1-1	6.165×10^{-1}	2.180×10^{-2}
		#1-2	6.366×10^{-1}	1.717×10^{-2}
		#1-3	6.241×10^{-1}	1.991×10^{-2}
	Electrode 2	#2-1	6.320×10^{-1}	2.370×10^{-2}
		#2-2	6.538×10^{-1}	2.476×10^{-2}
		#2-3	6.567×10^{-1}	2.657×10^{-2}
	Electrode 3	#3-1	6.931×10^{-1}	2.143×10^{-2}
		#3-2	6.834×10^{-1}	2.010×10^{-2}
		#3-3	6.567×10^{-1}	1.919×10^{-2}
	Mean ± s.d.		$(6.503 \pm 0.259) \times 10^{-1}$	$(2.163 \pm 0.292) \times 10^{-2}$
C-NCM	Electrode 1	#1-1	1.347×10^{-1}	3.669×10^{-3}
		#1-2	1.295×10^{-1}	2.493×10^{-3}
		#1-3	1.312×10^{-1}	2.920×10^{-3}
	Electrode 2	#2-1	1.376×10^{-1}	2.247×10^{-3}
		#2-2	1.503×10^{-1}	2.457×10^{-3}
		#2-3	1.510×10^{-1}	2.764×10^{-3}
	Electrode 3	#3-1	1.581×10^{-1}	2.446×10^{-3}
		#3-2	1.377×10^{-1}	4.139×10^{-3}
		#3-3	1.586×10^{-1}	3.376×10^{-3}
	Mean ± s.d.		$(1.432 \pm 0.112) \times 10^{-1}$	$(2.946 \pm 0.633) \times 10^{-3}$

Table S11 Initial discharge capacity and initial coulombic efficiency (ICE) of B-NCM and C-NCM cathodes at 0.1 C. Measurements were conducted using six independent half cells per sample (n = 6) at 25 °C within a voltage window of 3.0–4.3 V. The mean and standard deviation (s.d.) were calculated from all six measurements.

Sample	Cell ID	0.1C discharge capacity (mAh g^{-1})	ICE (%)
B-NCM	#1	203.2	84.1
	#2	201.8	83.9
	#3	204.2	84.0
	#4	202.5	84.0
	#5	202.3	84.2
	#6	202.0	84.1
	Mean ± s.d.	202.7 ± 0.9	84.1 ± 0.1
C-NCM	#1	213.0	86.2
	#2	215.3	86.6
	#3	212.0	85.5
	#4	211.8	86.6
	#5	211.3	86.3
	#6	212.8	86.6
	Mean ± s.d.	212.7 ± 1.4	86.3 ± 0.4

Table S12 R_f peak parameters obtained from DRT analysis of B-NCM and C-NCM cathodes at selected cycles. Peak parameters were extracted at the maximum of each DRT peak.

Sample	Cycle number	Frequency (Hz)	R_f (Ω)
B-NCM	1st	4.60×10^3	34.74
	100th	1.83×10^3	62.19
	200th	1.28×10^3	101.71
C-NCM	1st	1.88×10^4	9.85
	100th	5.10×10^3	27.65
	200th	2.31×10^3	49.92

Table S13 Calculation details for the volumetric energy density of a bilayer pouch-type full cell equipped with a dry-processed C-NCM electrode. The volumetric energy density was calculated based on the total cell volume, estimated from the total cell thickness and the anode electrode area.

Cell stack configuration		Anode | Separator | Cathode | Separator | Anode
Cathode	Type	Dry-processed electrode (double-sided)
	Composition	NCM : MWCNT : Super P : PVdF = 95 : 1.5 : 1.5 : 2 (wt.%)
	Dimension	9.0 cm^2 (3.0 × 3.0 cm^2)
	Areal capacity	8.1 mAh cm^{-2} (total, both sides)
Anode	Type	Slurry-cast electrode (single-sided)
	Composition	Graphite : Super P : SBR : CMC = 95 : 1 : 2 : 2 (wt.%)
	Dimension	10.24 cm^2 (3.2 × 3.2 cm^2)
Cell capacity (C_{cell})		72.9 mAh
Average discharge voltage (V_{avg})		3.754 V
Total energy (E_{tot})		0.274 Wh
Cathode thickness ($T_{cathode}$)		116 μm
Anode thickness (T_{anode})		120 μm
Separator thickness ($T_{separator}$)		20 μm
Package thickness ($T_{package}$)		105 μm
Total cell thickness (T_{tot})		361 μm
Volumetric energy density (based on total cell volume)		741 Wh L^{-1}

The volumetric energy density of the bilayer pouch-type full cell was calculated on a total cell volume basis using the following equation:

$$Volumetric\ energy\ density\ (Wh\ L^{-1}) = \frac{Total\ energy}{Total\ cell\ thickness \times Area} = \frac{E_{tot}}{T_{tot} \times A} = \frac{C_{cell} \times V_{avg}}{(T_{cathode} + T_{anode} + T_{separator} + T_{package}) \times A}$$

where $T_{cathode}$, T_{anode}, $T_{separator}$, and $T_{package}$ denote the thickness of the cathode (including the etched Al current collector), anode (including the Cu current collector), separator (PE), and pouch cell package, respectively. The area (A) was defined based on the anode electrode area.

Table S14 Calculation details for the specific energy density of a bilayer pouch-type full cell equipped with a dry-processed C-NCM electrode. The specific energy density was calculated based on both the cathode active material (CAM) mass and the total cell mass.

Cell stack configuration			Anode | Separator | Cathode | Separator | Anode	
Cathode	Type		Dry-processed electrode (double-sided)	
	Composition		NCM : MWCNT : Super P : PVdF = 95 : 1.5 : 1.5 : 2 (wt.%)	
	Dimension		9.0 cm^2 (3.0 × 3.0 cm^2)	
	Areal capacity		8.1 mAh cm^{-2} (total, both sides)	
Anode	Type		Slurry-cast electrode (single-sided)	
	Composition		Graphite : Super P : SBR : CMC = 95 : 1 : 2 : 2 (wt.%)	
	Dimension		10.24 cm^2 (3.2 × 3.2 cm^2)	
Cell capacity (C_{cell})			72.9 mAh	
Average discharge voltage (V_{avg})			3.754 V	
Total energy (E_{tot})			0.274 Wh	
Cathode composite mass (M_{cc})	0.365 g	Total cathode mass ($M_{cathode}$)		0.378 g
Al current collector mass (M_{Al})	0.013 g			
Anode composite mass (M_{ac})	0.320 g	Total anode mass (M_{anode})		0.460 g
Cu current collector mass (M_{Cu})	0.140 g			
Separator mass ($M_{separator}$)			0.020 g	
Electrolyte mass ($M_{electrolyte}$)			0.090 g	
Package mass ($M_{package}$)			0.080 g	
Total cell mass (M_{tot})			1.028 g	
Specific energy density	(based on CAM mass)		790 Wh kg^{-1}	
	(based on total cell mass)		267 Wh kg^{-1}	

The specific energy density of the bilayer pouch-type full cell was calculated on a total cell mass basis using the following equation:

$$Specific\ energy\ density\ (Wh\ kg^{-1}) = \frac{Total\ energy}{Total\ cell\ mass} = \frac{E_{tot}}{M_{tot}} = \frac{C_{cell} \times V_{avg}}{M_{cathode} + M_{anode} + M_{separator} + M_{electrolyte} + M_{package}}$$

where $M_{cathode}$, M_{anode}, $M_{separator}$, $M_{electrolyte}$, and $M_{package}$ denote the mass of the cathode (including the etched Al current collector), anode (including the Cu current collector), separator (PE), electrolyte, and pouch cell package, respectively.